

การศึกษาเปรียบเทียบการแก้ค่าการเบี่ยงรังสีโดยการปรับค่ากระแส-วินาทีจากเครื่องเอกซเรย์
คอมพิวเตอร์ในการตรวจกล้ำเนื้อหัวใจด้วยเครื่องสเปก: ศึกษาในหุ่นจำลอง



นางสาวชญาภา โคตรวิถี

ศูนย์วิทยทรัพยากร

จุฬาลงกรณ์มหาวิทยาลัย

วิทยานิพนธ์นี้เป็นส่วนหนึ่งของการศึกษาตามหลักสูตรปริญญาวิทยาศาสตรมหาบัณฑิต

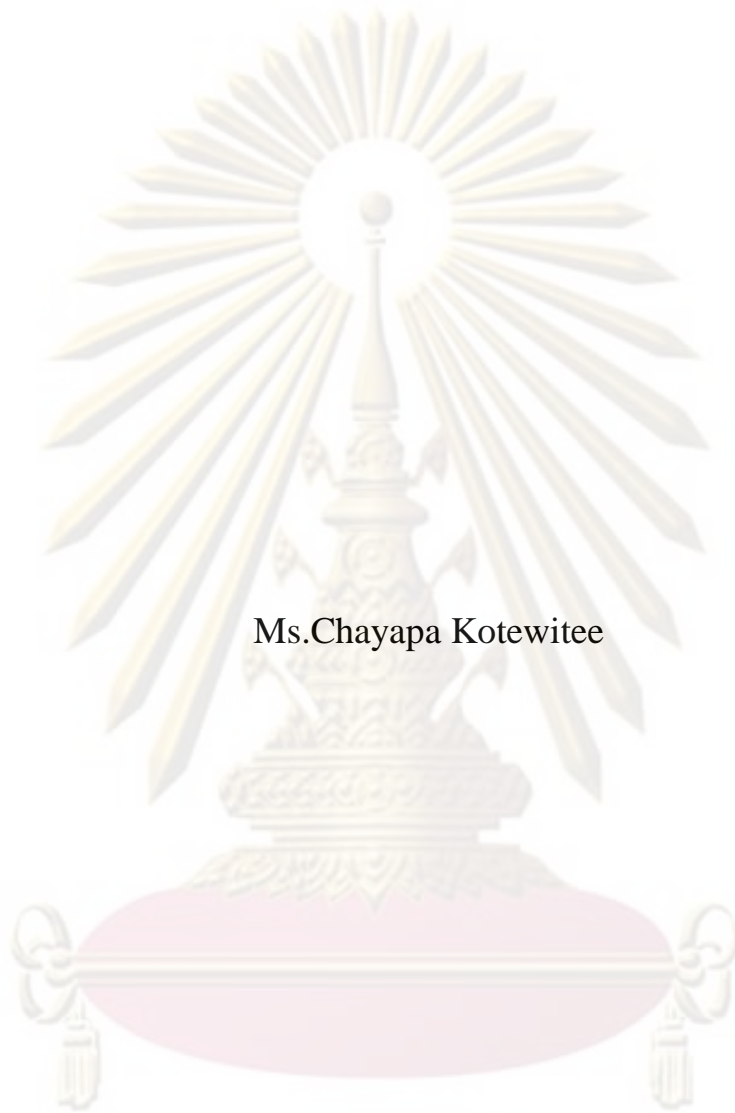
สาขาวิชาวิทยาศาสตร์ ภาควิชารังสีวิทยา

คณะแพทยศาสตร์ จุฬาลงกรณ์มหาวิทยาลัย

ปีการศึกษา 2552

ลิขสิทธิ์ของจุฬาลงกรณ์มหาวิทยาลัย

COMPARISON OF ATTENUATION CORRECTION BY VARIATION
OF TUBE CURRENT-TIME OF CT IN MYOCARDIAL
PERFUSION SPECT: A PHANTOM STUDY



Ms.Chayapa Kotewitee

ศูนย์วิทยทรัพยากร

A Thesis Submitted in Partial Fulfillment of the Requirements
For the Degree of Master of Science Program in Medical Imaging

Department of Radiology

Faculty of Medicine

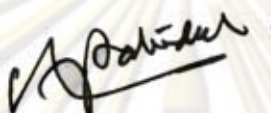
Chulalongkorn University

Academic Year 2009

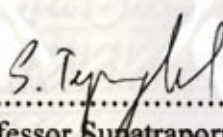
Copyright of Chulalongkorn University


Thesis Title COMPARISON OF ATTENUATION CORRECTION BY
 VARIATION OF TUBE CURRENT-TIME OF CT IN
 MYOCARDIAL PERFUSION SPECT: A PHANTOM
 STUDY
By Ms.Chayapa Kotewitee
Field of Study Medical Imaging
Thesis Advisor Associate Professor Thawatchai Chaiwatanarat, M.D.


Accepted by the Faculty of Medicine, Chulalongkorn University in Partial
Fulfillment of the Requirements for the Master's Degree

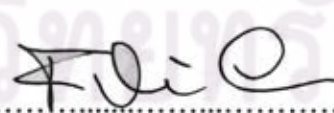

.....Dean of the Faculty of Medicine
(Professor Adisorn Patradul, M.D.)

THESIS COMMITTEE:


.....Chairman
(Associate Professor Supatraporn Thepmongkol, M.D.)


.....Thesis Advisor
(Associate Professor Tawatchai Chaiwatanarat, M.D.)


.....Thesis Co-Advisor
(Associate Professor Anchali Krisanachinda, Ph.D.)


.....External Examiner
(Professor Franco Milano, Ph.D.)

ศูนย์วิจัยทางการแพทย์
จุฬาลงกรณ์มหาวิทยาลัย

ชญาภา โคตรวิธิ : การศึกษาเปรียบเทียบการแก้ค่าการเบี่ยงรังสีโดยการปรับค่ากระแส-วินาทีจากเครื่องเอกซเรย์คอมพิวเตอร์ในการตรวจกล้ามเนื้อหัวใจด้วยเครื่องสเปก: ศึกษาในหุ่นจำลอง (Comparison of Attenuation Correction by Variation Tube Current-Time of CT in Myocardial Perfusion SPECT: A Phantom Study) อ.ที่ปรึกษาวิทยานิพนธ์หลัก, รศ.นพ.ชัชชัย ชัยวัฒน์รัตน์, 44 หน้า

การแก้ค่าการเบี่ยงรังสีเป็นวิธีที่ใช้เพื่อแก้ไขความผิดพลาดจากการแปลผลการตรวจกล้ามเนื้อหัวใจโดยวิธี scintigraphy และได้รับความนิยมเพิ่มขึ้นในปัจจุบัน วิธีการนี้จะทำให้การวินิจฉัยโรคมีความแม่นยำและคุณภาพของภาพกล้ามเนื้อหัวใจดีขึ้น ในปัจจุบันเครื่องมือที่ใช้เป็นสองระบบรวมกัน คือ SPECT/CT โดยใช้เอกซเรย์คอมพิวเตอร์ในการแก้สร้างภาพแผนที่การเบี่ยงรังสีเพื่อนำไปแก้ไขซึ่งใช้เวลาสั้นๆและให้ลักษณะทางกายวิภาคของความผิดปกติได้ดีขึ้น การศึกษานี้มีวัตถุประสงค์เพื่อศึกษาผลของการแก้ค่าการเบี่ยงรังสีเมื่อปรับค่ากระแส-วินาทีของเครื่องเอกซเรย์คอมพิวเตอร์ของการตรวจกล้ามเนื้อหัวใจซึ่งศึกษาในหุ่นจำลองเครื่องมือที่ใช้คือเครื่อง SPECT/CT ผลิตภัณฑ์ของบริษัทซิเมนต์ รุ่น Symbia T6 จากประเทศเยอรมัน เครื่องดังกล่าวได้นำสองระบบมารวมกันคือ SPECT detector และ เครื่องเอกซเรย์คอมพิวเตอร์ 6 สไลด์ การศึกษานี้ใช้หุ่นจำลองคล้ายมนุษย์ที่มีตับ ปอด หัวใจและ กระดูกสันหลังรวมอยู่ภายในลำตัวส่วนอก ภายในปอดใส่เม็ดโพรหมและน้ำเพื่อจำลองความหนาแน่นของปอด หัวใจจำลองความปกติและผิดปกติของค่านับวัดในกล้ามเนื้อหัวใจ การศึกษาแรกเป็นการศึกษาในหุ่นจำลองหัวใจที่ไม่ใส่ความผิดปกติโดยปรับเปลี่ยนค่ากระแส-วินาที 5 ค่า คือ mAs 34, 43-48, 100, 150 และ 200 เพื่อศึกษาผลต่อความสม่ำเสมอของภาพกล้ามเนื้อหัวใจหลังจากแก้ค่าการเบี่ยงรังสีแล้ว จากนั้นจึงศึกษาถึงผลของการปรับเปลี่ยนค่ากระแส-วินาที 3 ค่า คือ 34, 43-48 และ 200 ที่มีต่อความคมชัดของภาพโดยการเปลี่ยนลักษณะของความผิดปกติในหุ่นจำลองหัวใจคือ ขนาด, ตำแหน่งต่างๆในผนังหัวใจและปริมาณความเข้มข้นของสารรังสีในความผิดปกติ ผลการศึกษาพบว่าไม่มีความแตกต่างกันอย่างมีนัยสำคัญของความสม่ำเสมอของภาพสำหรับการใช้ค่ากระแส-วินาที 4 ค่าสูงคือ 43-48, 100, 150 และ 200 แต่ทั้ง 4 ค่าให้ ความสม่ำเสมอของภาพ ดีกว่าการใช้ค่ากระแส-วินาที 34 อย่างมีนัยสำคัญ สำหรับการศึกษ ความคมชัดของภาพ แสดงให้เห็นว่า มีความแตกต่างกันอย่างมีนัยสำคัญระหว่างความเข้มข้นของสารรังสี 25% กับ 75% แต่สำหรับความแตกต่างของขนาดของความผิดปกติคือ 1×1.5 ซม.² และ 1×2 ซม.² ไม่มีผลต่อ ความคมชัดของภาพในทำนองเดียวกันไม่ว่าความผิดปกติจะอยู่ในตำแหน่งใดของผนังกล้ามเนื้อหัวใจก็ไม่มีผลต่อ ความคมชัดของภาพทั้งสิ้น แม้ว่าจะใช้ค่ากระแสวินาทีที่เปลี่ยนไป จึงสรุปได้ว่าค่ากระแส-วินาทีต่ำๆจะทำให้ได้ ความสม่ำเสมอของภาพที่ต่ำ อย่างไรก็ตามก็ใช้ค่ากระแส-วินาทีขนาด 43-48 ให้ภาพที่มีคุณภาพดีเทียบเท่ากับการใช้ค่ากระแส-วินาทีที่สูงขนาด 200 ดังนั้นค่ากระแส-วินาทีขนาด 43-48 จึงน่าจะเป็นค่าที่เหมาะสมที่สุดในการนำมาใช้ตรวจผู้ป่วยเนื่องจากให้ปริมาณรังสีต่อผู้ป่วยต่ำกว่า

จุฬาลงกรณ์มหาวิทยาลัย

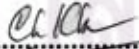
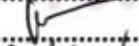

ภาควิชา.....รังสีวิทยา.....ลายมือชื่อนิสิต.....*Ch. Ch.*
 สาขาวิชา.....จักษุเวชศาสตร์.....ลายมือชื่อ อ.ที่ปรึกษาวิทยานิพนธ์หลัก.....
 ปีการศึกษา.....2552.....ลายมือชื่อ อ.ที่ปรึกษาวิทยานิพนธ์ร่วม.....*สม. ม.พ.*

5174768030: MAJOR MEDICAL IMAGING

KEYWORDS: ATTENUATION/SPECT/CT/ MYOCARDIAL PERFUSION

CHAYAPA KOTEWITEE: COMPARISON OF ATTENUATION CORRECTION BY VARIATION OF TUBE CURRENT-TIME OF CT IN MYOCARDIAL PERFUSION SPECT: A PHANTOM STUDY. THESIS ADVISOR: ASSOC. PROF. TAWATCHAI CHAIWATANARAT, M.D., 44 pp.

Attenuation correction is the method to improve error of myocardial perfusion scintigraphy interpretation and is increasing used nowadays. The methods had demonstrated improved diagnostic accuracy and quality of myocardial perfusion SPECT images. Recently SPECT-CT hybrid instrument which obtain statistically rich of x-ray transmission scan in a very short time solve many of the issues associated with radioisotope-based attenuation correction methods and afford better anatomic localization of abnormal radiopharmaceutical accumulations. This research objective is to study the effect of attenuation correction by varying the x-ray tube current-time, in myocardial perfusion phantom. The SPECT/CT system used in this study is manufactured by Siemens Medical Solutions, Symbia T6 Model, Germany. The system integrates the SPECT detectors, with a 6 multi-slice CT scan. Anthropomorphic phantom (Model ECT/TOR/P, Data Spectrum Corporation) used in this study includes liver, lung, heart and spine inserts. Lung inserts filled with Styrofoam beads and water to simulate lung tissue density. Cardiac insert (Model ECT/CAR/I, Data Spectrums Corporation) simulates normal and abnormal uptake in myocardium. First we studied the effect of 5 different tube current-time of CT scan i.e. 34, 43-48, 100, 150 and 200, on the uniformity of attenuation corrected myocardial perfusion phantom images. Then effects of 3 different tube current-time i.e. 34, 43-48 and 200 on image contrast were selected with varying defect size, location and activity concentration. The results show that the uniformity of the images acquired by mAs 43-48, 100, 150 and 200 do not significantly differ but significantly better than those acquired by mAs 34. The image contrast studies show that the activity concentration of 25% and 75% results in significant difference of the contrast of the image. But the difference of defect size between 1×1.5 and 1×2 cm² has no significant effect on image contrast. And also there is no significant difference of percent contrast of lesion using different tube current-time on the same defect size and activity concentration matter what location of the defect is. In conclusion, low tube-current time results in low uniformity of the attenuation corrected image. However, the value of mAs 43-48 gives comparable image quality as the high tube-current time of 200 and is the preferable choice because of the lower radiation dose to patient.

Department:	Radiology	Student's Signature	
Field of Study:	Medical Imaging	Advisor's Signature	
Academic Year:	2009	Co-Advisor's Signature	

ACKNOWLEDGEMENTS

The success of this thesis depends on the contributions of many people. In particular, I wish to express gratitude and deepest appreciation to Associate Professor Tawatchai Chaiwatanarat M.D., Nuclear Medicine Division, Department of Radiology, Faculty of Medicine, Chulalongkorn University, my major advisor, for his supervision, guidance, encouragement and invaluable advice during the whole study. I am also express gratitude and appreciation to Associate Professor Anchali Krisanachinda and Mr. Panya Pasawang, Nuclear Medicine Division, King Chulalongkorn Memorial Hospital, Thai Red Cross Society, my co-advisor for they help in the experiment, assistance and suggestion for this work. I would like to greatly thank Radiological Technologist, Nuclear Medicine Division, King Chulalongkorn Memorial Hospital, Thai Red Cross Society, especially, Mr.Tanawat Sontrapornpol, Mr.Chatchai Navikhachewin, for their help and suggestion in this research. I would like to deeply thank Associate Professor Anchali Krisanachinda, Nuclear Medicine Division, Department of Radiology, Faculty of Medicine, Chulalongkorn University and Professor Franco Milano, Florence University, Italy, for their comments and suggestions in this work. I am also thankful for all teachers, lecturers and staff in the Master of Science Program in Medical Imaging, Faculty of Medicine, Chulalongkorn University, for their unlimited teaching of knowledge throughout whole study in Medical Imaging.

Finally, my grateful is forwarded to the support by Thai Red-Cross Society, King Chulalongkorn Memorial Hospital, Global Medical Solution (Thailand) for the partial support in radiopharmaceutical. Last but not least I wish to thank the Nuclear Medicine Staff at King Chulalongkorn Memorial Hospital for their encouragement through the graduate studies.



ศูนย์วิทยทรัพยากร
จุฬาลงกรณ์มหาวิทยาลัย

CONTENTS

	Page
ABSTRACT (THAI).....	iv
ABSTRACT (ENGLISH).....	v
ACKNOWLEDGEMENTS.....	vi
CONTENTS.....	vii
LIST OF TABLES.....	x
LIST OF FIGURES.....	xi
LIST OF ABBREVIATIONS.....	xii
CHAPTER I INTRODUCCION	1
1.1 Background and rationale.....	1
1.2 Research objectives.....	1
1.3 Definitions.....	2
CHAPTER II REVIEW OF RELATED LITERATURES	3
Overview of myocardial perfusion SPECT.....	3
2.1 Principle of cardiac SPECT.....	3
2.2 SPECT collimator and detector.....	4
2.3 Data acquisition.....	5
2.4 Photon attenuation.....	5
2.4.1 X-ray transmission scan.....	6
2.5 Scatter correction.....	8
2.6 Tomographic reconstruction.....	9
2.6.1 Filtered backprojection.....	9
2.6.1.1 The convolution method.....	10
2.6.1.2 The Fourier method.....	11
2.6.2 Iterative algorithm.....	11
2.7 Quantitative analysis.....	11
2.8 Computed tomography.....	12
2.8.1 Principle of CT.....	12
2.8.2 SPECT/CT.....	13

	Page
2.9 Review of related literatures.....	14
CHAPTER III RESEARCH METHODOLOGY.....	15
3.1 Research design.....	15
3.2 Research design model.....	15
3.3 Conceptual framework.....	16
3.4 Research question.....	16
3.5 Research objective.....	16
3.6 Key words.....	16
3.7 The sample.....	16
3.8 Materials.....	17
3.8.1 Single Photon Emission Computed Tomography/Computed Tomography.....	17
3.8.2 Antropomorphic SPECT phantom.....	17
3.8.3 Technetium pertechnetate ($^{99m}\text{TcO}_4^-$).....	18
3.9 Methods.....	18
3.9.1 SPECT/CT daily QC.....	18
3.9.2 Phantom preparation.....	18
3.9.3 SPECT/CT procedure.....	19
3.9.4 Data collection.....	20
3.10 Statistical analysis.....	20
3.11 Ethical considerations.....	20
3.12 Expected benefits.....	20
CHAPTER IV RESULTS.....	21
4.1 The percent normalize value.....	21
4.2 The percent contrast of lesion.....	22
CHAPTER V DISCUSSION AND CONCLUSIONS.....	25
5.1 Discussion.....	30
5.2 Conclusions.....	31
REFERENCES.....	32

	Page
APPENDICES	33
Appendix A: Case record form.....	34
Appendix B: Performance measurements of Single Photon Emission Computed Tomography.....	35
VITAE	44



ศูนย์วิทยทรัพยากร
จุฬาลงกรณ์มหาวิทยาลัย

LIST OF TABLES

Table		Page
2.1	CT number for number of tissue	7
3.1	CT scan parameters for mediastinum SPECT/CT scan.....	19
4.1	Attenuation correction in each wall of myocardium.....	21
4.2	The comparison of percent normalization value by paired t-test	21
4.3	The percent contrast of lesion size 1x1.5cm ²	24
4.4	The percent contrast of lesion size 1x2cm ²	25
4.5	The comparison of percent contrast of lesion by paired t-test at 25% lesion concentration of myocardium and lesion size 1x1.5cm ²	27
4.6	The comparison of percent contrast of lesion by paired t-test at 50% lesion concentration of myocardium and lesion size 1x1.5cm ²	27
4.7	The comparison of percent contrast of lesion by paired t-test at 25% lesion concentration of myocardium and lesion size 1x1.5cm ²	27
4.8	The comparison of percent contrast of lesion by paired t-test at 25% lesion concentration of myocardium and lesion size 1x2 cm ²	28
4.9	The comparison of percent contrast of lesion by paired t-test at 50% lesion concentration of myocardium and lesion size 1x2 cm ²	28
4.10	The comparison of percent contrast of lesion by paired t-test at 75% lesion concentration of myocardium and lesion size 1x2 cm ²	28
4.11	The comparison of percent contrast of lesion by paired t-test in different lesion size.....	29



 ศูนย์วิทยทรัพยากร
 จุฬาลงกรณ์มหาวิทยาลัย

LIST OF FIGURES

Figure		Page
2.1	Energy spectrum with triple windows to estimate scatter distribution.....	8
2.2	3 Myocardial perfusion short-axis, left without attenuation correction, middle with attenuation correction, right with scatter and attenuation correction	9
2.3	Simple backprojection method,filter backprojection method.....	10
3.1	Research design model.....	15
3.2	Conceptual framework.....	16
3.3	Single Photon Emission Computed Tomography/ Computed Tomography (SPECT/CT).....	17
3.4	Insert cardiac chamber	17
3.5	Anthropomorphic SPECT Phantoms.....	18
3.6	Lesion size	19
4.1	Bull's eye map of defect free phantom in different tube current-time.....	22
4.2	The compare percent normalization value	22
4.3	Bull's eye map of lesion size $1 \times 1.5 \text{ cm}^2$, 75 % lesion concentration in different tube current-time.....	22
4.4	Bull's eye map of lesion size $1 \times 1.5 \text{ cm}^2$, 50 % lesion concentration in different tube current-time.....	23
4.5	Bull's eye map of lesion size $1 \times 1.5 \text{ cm}^2$, 25 % lesion concentration in different tube current-time.....	23
4.6	Bull's eye map of lesion size $1 \times 1.5 \text{ cm}^2$ and $1 \times 2 \text{ cm}^2$	23
4.7	The compare percent contrast of lesion in different tube current-time at $1 \times 1.5 \text{ cm}^2$	26
4.8	The compare percent contrast of lesion in different tube current-time at $1 \times 2 \text{ cm}^2$	26



ศูนย์วิทยทรัพยากร
 จุฬาลงกรณ์มหาวิทยาลัย

LIST OF ABBREVIATIONS

Abbreviation	Terms
\approx	Approximate
Z	Atomic number
AEC	Automatic Exposure Control
AC	Attenuation Correction
cm ³	Cubic centimeter
COR	Center of rotation
cps	Count per second
CT	Computed Tomography
FOV	Field of view
FWHM	Full width at half-maximum
g	Gram
hr	Hour
HU	Hounsfield units
IEC	International Electric Commission
keV	Kiloelectronvolt
kVp	Kilovoltage peak
mA	Milliamperere
mAs	Milliamperere-second
MBq	Megabecquerel
MeV	Megaelectronvolt
mL	Milliliter
μ Ci	Micro curies
μ	Micro

Abbreviation	Terms
NEMA	National Electrical Manufacturers Association
%	Percent
PMTs	Photomultiplier tubes
NaI	Sodium iodide
SPECT	Single Photon Emission Computed Tomography
$^{99m}\text{TcO}_4^-$	Technetium pertechnetate



ศูนย์วิทยทรัพยากร
จุฬาลงกรณ์มหาวิทยาลัย

CHAPTER I

INTRODUCTION

1.1 Background and rationale

Single Photon Emission Computed Tomography (SPECT) is noninvasive imaging modalities for diagnosis and managing patients with coronary diseases. [1] Attenuation is the most important factor influence the normal pattern of perfusion in SPECT studies. Breast tissue and left hemidiaphragm are the most frequently identified sources of attenuation. Therefore, most notable soft tissue attenuation should be eliminated. American Society of Nuclear Cardiology and Society of Nuclear Medicine recommended the incorporation of attenuation correction to improve the diagnostic accuracy. [2]

Attenuation correction is not common methods for application of myocardial perfusion SPECT. Attenuation correction method using an external line source of an isotope with a long half-life, such as gadolinium-153 (^{153}Gd) that rotates on the opposite side of the patient from the camera detector during SPECT imaging, producing a transmission image as the external photon pass through the patient. This image resembles a poor quality CT scan, but the data are good enough to perform attenuation correction when applied to the emission image of the organ of interest, such as the heart. Depending on the difference between the photon energies of the radioisotopes used, the emission and transmission images may be obtained simultaneously by using two different pulse-height windows. Recently SPECT-CT hybrid instruments which obtain statistically rich of x-ray transmission scan in a very short time solve many of the issues associated with radioisotope-based attenuation correction methods and afford better anatomic localization of abnormal radiopharmaceutical accumulations.

The CT based attenuation correction method can be successfully implemented with clinical cardiac SPECT protocols. It has been attempted to use CT for anatomic image imported and produce high photon flux to correct images slice by slice, but it is difficult to correct matching of morphologic and scintigraphic data sets since images are acquired on different time point.

The detectability of myocardial perfusion depends on lesion size, lesion location and lesion concentration. Low dose CT is most frequency used for examination but can only be reduced the patient dose to levels at which the detectability of relevant details is not unduly affected by increase noise. Anatomical regions which are characterized by large differences in X-ray transmission is therefore these application best suited for low dose CT.

1.2 Research objectives

1. To determine the uniformity of attenuation corrected SPECT image using various tube current-time of CT in myocardial perfusion SPECT phantom.
2. To determine the defect detectability of attenuation corrected SPECT image using various tube current-time of CT and various defect inserted parameter, i.e. size, location and activity concentration, in myocardial perfusion SPECT phantom.

1.3 Definitions [3]

Attenuation correction

Attenuation is the phenomenon of weakening the radiation emanating from an organ on its way to the detector. SPECT reconstruction can hide evidence of an attenuation artifact that influences a projection or set of projections in a major manner or it can magnify a relatively minor problem into a significant concern.

Computed Tomography

A technique for constructing images of the structures at a particular depth within the body done by taking several x-ray images at different angles and then using a computer to reconstruct and analyze the resulting images.

Microcurie

The microcurie is a unit of radioactivity, defined as $1 \mu\text{Ci} = 3.7 \times 10^4$ disintegrations per second = 2.22×10^6 disintegrations per minute.

Single Photon Emission Computed Tomography

A modality generates images depicting the distributions of photon emitting nuclides in patients.

Tube Current-time (mAs)

An X-ray tube is a vacuum tube that produces X-rays. The vacuum tube, there is a cathode which emits electrons into the vacuum and an anode to collect the electrons, thus establishing a flow of electrical current. In applications, the current represent in term of mA is able to be pulsed on millisecond or second that call tube current-time (mAs).



ศูนย์วิทยุทรัพยากร
จุฬาลงกรณ์มหาวิทยาลัย

CHAPTER II

REVIEW OF RELATED LITERATURES

Overview of myocardial perfusion SPECT

Myocardial perfusion single photon emission computed tomography (SPECT) is a widely utilized noninvasive imaging modality for the diagnosis and management of coronary artery diseases. Physical interaction of photon in the patient by Compton scattering or photoelectric effect and the effect of spatial resolution by collimator detector are significant factors affecting the quality of SPECT images, importance to cardiac SPECT.

2.1 Principle of cardiac SPECT [3]

Conventional gamma cameras provide two dimensional planar images of three-dimensional objects. Structural information in the third dimension, depth is obscured by superimposition of all data along this direction. Although imaging of the object in different projections can give some information about the depth of the structure, precise assessment of the depth of a structure in an object is made by tomographic scanners. The prime of these scanners is to display the images of the activity distribution in different sections of the object at different depths.

The initial approach to the tomographic technique was to focus the image of the object at the plane of interest and at the same time to blur the images of the object not in plane. This is called the focal plane method or longitudinal tomography. Focused collimators are used to obtain images of the objects at the focal plane. Seven-pinhole collimators and slant-hole collimators have been used in longitudinal tomography to provide longitudinal section images. However, even through out of focus plane images are blurred, in focus plane images also are obscured by counts from the former. Furthermore, because the imaging device is not rotated around the patient, only a limited number of angular views are available, as projected by the collimator holes. An improvement over focal plane tomography has been made by introducing transverse tomography, in which multiple views are obtained at many angles around the patient. This method is called emission computed tomography (ECT), which is based on many mathematical algorithms. ECT provides images at distinct focal plane of the object. In nuclear medicine, two types of ECT have been in practice base on the type of radionuclide used, Single Photon Emission Computed Tomography (SPECT) and Positron Emission Tomography (PET). The most common, SPECT system consists of a typical gamma camera with one to three NaI(Tl) detector heads mounted on a gantry, an on-line computer for acquisition and processing of data and display system. The detector head rotates around the long axis of the patient at small angle increment for 180° to 360° angular sampling. The data are collected at each angular position and normally stored in a 64x64 or 128x128 matrix in the computer for later reconstruction of the image of the plane of interest. Transverse (short axis), sagittal (vertical long axis) and coronal (horizontal long axis) images can be generated from the collected data. Multihead gamma camera collect data in several projections simultaneously and thus reduce the time of imaging.

The SPECT is largely derived from the three-dimensional nature of its images compared with the two dimensional projection of planar perfusion imaging. Whereas planar image values are composed of the superposition of attenuated activity from

source along a line through the patient, SPECT permits three-dimensional interaction assessment of the perfused volume. Regional and global perfusion pattern as well as cardiac shape information. Tomography permits separation of target region from overlying structures. It is primarily attributed associated with improved diagnosis result over planar image and quantitation in early clinical study and the broad acceptance of this imaging modality clinically. An important quantity related to the diagnostic value is the target to background ratio. Quantitative myocardial perfusion and function is greatly improved as algorithms can be directed to analyze image data more directly associated with the heart.

2.2 SPECT Collimator and detector

SPECT detector is required to localize the line of emission of photons for tomographic reconstruction. This is achieved at great cost to system sensitivity as only a few percent of the photon are emitted in a direction that will permit detection. Collimators are typically constructed of lead or similar material with high atomic number, which act as good absorbers of photons. Several geometries have been proposed for cardiac SPECT collimation including parallel, convergent and asymmetric array. Most systems utilize parallel hole or convergent geometry in the form of fan beam or an asymmetric fan beam. The geometry and specification of the array determine the effect on system sensitivity. The major factor influencing is spatial resolution. The geometric influence collimator on system spatial resolution is two to four times that of intrinsic component. A fundamental principle of collimator is trade off between system sensitivity and spatial resolution. This has important implications for SPECT image quality as the orbit about the patient cause the detector to be, at time, at different distance from the organs. Collimators are characterized by the hole length, diameter, number of the hole per unit area and septal thickness. Higher resolution collimator tends to have longer hole length and smaller bore. High energy collimation has large thick septa to minimize penetrate of high energy photons. Increase the hole length or reducing the bore, decrease the solid angle through which photon emitted from a point in the patient can reach the detector, thereby reducing sensitivity. Photon that are incident on the septa are largely absorbed for the low energy used in cardiac SPECT, although a small percentage may penetrate the septa leading to an increase of FWTM value. Amount of septa penetration increase with increase photon energy and therefore, reduced contrast resolution can be expected with higher energy tracer.

As the distance of source to the detector increases, spatial resolution decreases. Distance dependent spatial resolution is the result of the collimator geometry and contributes to an inconsistency in the projection as the heart is at different distance from the detector to patient. The reconstructed image is a weighted composite of these different spatial resolution values. SPECT orbit may be broadly classified as circular and non circular, including elliptical and other eccentric orbits. With the circular orbits, the detector is at fixed distance from the center of rotation for all angles. The heart is on average farther from the detector over all the projection angles, leading to reduced spatial resolution but less variability with angular projection. Noncircular orbits can at time be closer to the heart for some views and therefore have improved spatial resolution for these views. This is obtained at the expense of increased variability in spatial resolution, which is a potential source of artifacts. Circular orbits have been recommended by the American Society of Nuclear Cardiology guidelines but noncircular may be required for attenuation correction

methods to prevent body truncation. Perhaps most important is that consistent approach to orbits selection be used. Component of SPECT studies should utilize the same orbital type and repeat studies on the same patient should attempt to be acquired with the same orbits. If not, orbital variation should be taken into consideration during interpretation.

2.3 Data acquisition [4]

Data acquired by rotating the detector head around the long axis of the patient over 180° or 360°, while 180° data collection is commonly used for cardiac study, since it minimizes the effects of attenuation and variation of resolution with depth. Data collection can be made in either continuous motion or step-and-shoot mode. In continuous acquisition, the detector rotate continuously at a constant speed around the patient, and the acquired data are later binned into the number of segments equal to the number of projection desired. In the step-and shoot mode, the detector moves around the patient at selected incremental angles and collects the data for the projection at each angle.

The predominant acquisition orbits for cardiac perfusion SPECT has become the 180-degree right anterior oblique-left posterior oblique orbit, although 360-degree orbits were promoted in early investigation. The relative merit of these two approach was debated early in the development of SPECT and the use of 180 degree acquisition has been largely influenced by the predominant development of dual 90-degree detector systems. Improved defect contrast and signal to noise value are obtained with 180-degree orbits. This is attributed to the poor spatial resolution of the posterior views where the heart is further from the detector and the additional scatter and attenuation from these views, both of which degrade image quality. Reconstructed images from 180-degree orbits are reported to have a slight distortion in the transverse plane attributable to variable spatial resolution and nonuniform attenuation by the thorax. With 360-degree orbits, spatial resolution is reduced compared with 180-degree acquisition, as the opposing view is combined in the reconstruction, forming an effective resolution equal to the geometric mean of the two values. This operation yield spatial resolution that is less variable across the transverse plane. Despite these considerations, 180-degree acquisition has become the standard for cardiac SPECT imaging, particularly for dual detector 90-degree systems.

2.4 Photon attenuation

Gamma ray photons are attenuated in body tissue while passing through a patient. Distortion in count density on the image cause from attenuation. The degree of attenuation depends on the photon energy, the thickness of tissue and the linear attenuation coefficient of the photons in tissue. Techniques are employed to correct for attenuation. In one method, an uncorrected image is taken and the thickness of tissue through which the photons are attenuated is estimated. Using constant linear attenuation coefficient for the photon in the tissue, each pixel data is correct to this equation to reconstruct the image.

$$I_t = I_0 e^{-\mu x} \quad (2.1)$$

If the photon beam of initial intensity I_0 passes through an absorber of thickness x , then the transmitted beam I_t is given by exponential equation, where μ is the linear attenuation coefficient of absorber for photon of interest and has unit of

cm^{-1} . The factor of $e^{-\mu x}$ represents the factor of the photon transmitted. In another technique, a phantom simulating the organ of interest is used to generate correction factors, which are then applied to data acquired in real imaging of an object. Assumption of a constant linear attenuation coefficient can be useful for symmetric organs with similar tissue density, and it is not valid for several organs such as the heart, cause of the close proximity to another organs. Gamma ray traversing different thicknesses of various body tissues may be detected within the photopeak and therefore a constant correction factor may not be sufficient for attenuation correction. Attenuation corrections are not applied to SPECT images for reasons of complexity of the problem. Currently, SPECT system used a transmission source of a radionuclide that is mounting opposite to detector much like an x-ray tube in computed tomography (CT). The detectors collect the transmission data to correct for attenuation in emission data. For $^{99\text{m}}\text{Tc}$ imaging, common transmission source are gadolinium-153 (^{153}Gd) (48keV, 100keV) and ^{57}Co (122keV), for thallium imaging, americium-241 (^{241}Am) (60keV), which ^{153}Gd and ^{57}Co are mostly used. A well-collimated line source is mount that is translated across the plane parallel to the detector face to collect transmission data. The line source is scanned at each angular stop used during the SPECT data collection. The transmission and emission photons have different energies, it is possible that these configuration of SPECT system can be used to collect both transmission and emission data simultaneously using separate discriminator setting. However, one should keep in mind that there is a likelihood of spillover of scattered high energy photon into the low energy photopeak window. The transmission data are used to calculate the attenuation factor to apply to emission data.

2.4.1 X-Ray Transmission Scanning [5]

Attenuation maps generated for attenuation correction of the radionuclide image have been traditionally obtained using an external radionuclide source. This process is identical conceptually to the process of generating a CT image with an x-ray tube that transmits radiation through the body, with the transmitted intensity recorded by an array of detector elements. The transmission data can then be reconstructed using a tomographic algorithm that inherently calculates the attenuation coefficient at each point in the reconstructed slice. The CT image is represented in terms of normalized CT numbers or Hounsfield units; CT image contains pixel values that are related to the linear attenuation coefficient at that point in the patient, calculated for the mean energy of the x-ray photons used to generate the CT image. After the computer calculates the linear attenuation coefficient for each pixel via filtered back projection, the values are normalised to the value for water as a reference, scaled and presented as a Hounsfield or CT-number (H) which is defined as:

$$H = 1000 \frac{\mu_m - \mu_{\text{water}}}{\mu_{\text{water}}} \quad (2.2)$$

where μ_m and μ_{water} are the linear attenuation coefficients for the tissue material and for water, respectively. The CT-number of water is therefore zero. CT-numbers for a number of tissues are shown in the following table 2.1

Table 2.1 CT-number for number of tissue

Tissue	CT number (H)
Lung	-300
Fat	-90
White Matter	30
Gray Matter	40
Muscle	50
Trabecular Bone	300-500
Cortical Bone	600-3,000

Therefore, it is not surprising that CT can generate a patient-specific attenuation map for correcting the radionuclide image for photon attenuation. In a clinical setting, this can be performed by scanning the patient in the CT scanner and then moving the patient to a SPECT system for acquisition of the radionuclide data. A challenging problem occurs because the x-rays and radionuclide data must be registered spatially with the CT-derived attenuation map for reconstruction. The image registration can be performed by acquiring both the x-ray and the radionuclide images of the patient with fiducially markers that can be identified to align the images using off-line image registration software. These image registration techniques have been relatively successful for imaging the head, and to a lesser degree for imaging the pelvis, both of which are constrained geometrically by the skeleton. However, off-line image registration is more difficult to perform accurately in the thorax, abdomen, and head and neck regions where the body can flex and bend, making it difficult to maintain a consistent anatomic configuration when the x-rays and radionuclide data are acquired during separate imaging sessions on different scanners. Recently, dual-modality imaging systems have been developed that incorporate radionuclide imaging with CT in a single system. The dual-modality systems have an integrated patient table that allows both the x-ray and the radionuclide images to be acquired without removing the patient from the system. This allows the x-ray and radionuclide images to be acquired with a consistent patient geometry and with a minimal level of patient movement, thereby facilitating the coregistration of the CT image with SPECT image. The ability of the dual-modality imaging systems to facilitate image fusion is seen as an important advance, especially for anatomic localization of radiopharmaceutical uptake for tumor staging and for treatment planning in oncologic studies. In addition, the CT image obtained with a dual-modality system can be used to generate a patient-specific attenuation map for attenuation correction of the radionuclide data. As noted above, CT inherently provides a patient-specific measurement of the linear attenuation coefficient at each point in the image. However, the linear attenuation coefficient measured with CT is calculated at the x-ray energy rather than at the energy of the photon emitted by the radiopharmaceutical acquired during the radionuclide imaging study. It is therefore necessary to convert the linear attenuation coefficients obtained from the CT scan to those corresponding to the energy of the emission photons used for the radionuclide imaging study. The SPECT/CT systems have developed similar methods for calibrating the CT image for attenuation correction of the emission data.

2.5 Scatter correction [6]

As indicated in the introduction, Compton scatter is part of the attenuation process, however, scatter is normally considered to be a separate problem. When a gamma ray passes through tissue the photon is not necessarily completely stopped but may be scattered. Scattered photons are diverted from their original path with some loss in energy. The purpose of the energy window on the gamma camera is to reduce the number of these scattered events that are detected. However there are still many of the detected photons with energy within the photopeak that have undergone scatter and these can lead to artifacts in the reconstruction as well as loss of contrast. It should be noted that in some studies approximately 30% of detected counts in SPECT have undergone Compton scatter. The problem is particularly complex where there is non-uniform attenuation. In effect scatter appears to be a greater problem when attenuation correction is performed. There have been many methods of scatter correction suggested and this is still a topic for continuing research. Unfortunately there is no single method that is universally accepted, although possibly the methods that is most widely used are the triple energy window or dual energy window methods. Other groups have developed alternative approaches including use of multiple energy windows, convolution subtraction or more complex scatter modeling. The triple energy windows approach involves acquisition of additional images using energy windows either just below or on each side of the photopeak. The assumption is that scatter recorded in these windows will be similar to the scatter in the photopeak. Therefore the scatter in the photopeak can be estimated by subtraction. (See Figure 2.1) If the two narrow windows have width, w , and the photopeak width, p , then the scatter is estimated as:

$$\text{Scatter} = (\text{sum of counts in narrow windows} / 2) * p/w \quad (2.2)$$

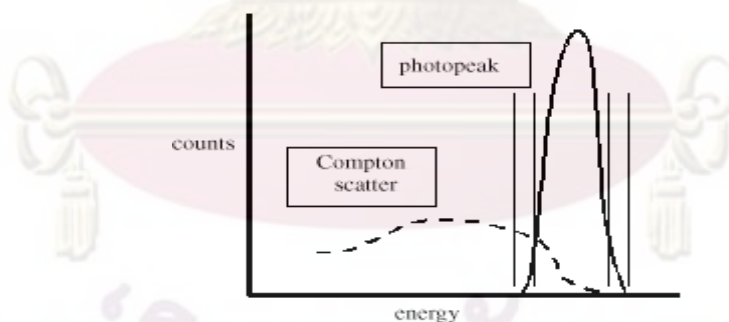


Figure 2.1 Energy spectrum with triple windows to estimate scatter distribution

The technique has several advantages over alternative methods since it is simple to apply and directly measures scatter (both number of counts and spatial distribution). On the negative side, the subtraction results in enhanced noise unless care is taken to smooth the scatter estimate. An alternative approach that improves the noise quality is to utilize the scatter estimate within an iterative reconstruction algorithm.

Scatter correction results in improvement in image contrast and it is essential if absolute quantification is desired. However for most clinical cases, e.g. brain, contrast enhancement can be achieved by display thresholding and the value of scatter

correction is questionable. In cardiac studies, performing attenuation correction alone tends to result in reduction of contrast compared with results without attenuation correction. As a result some form of scatter correction is desirable to restore visual contrast (Figure 2.2).

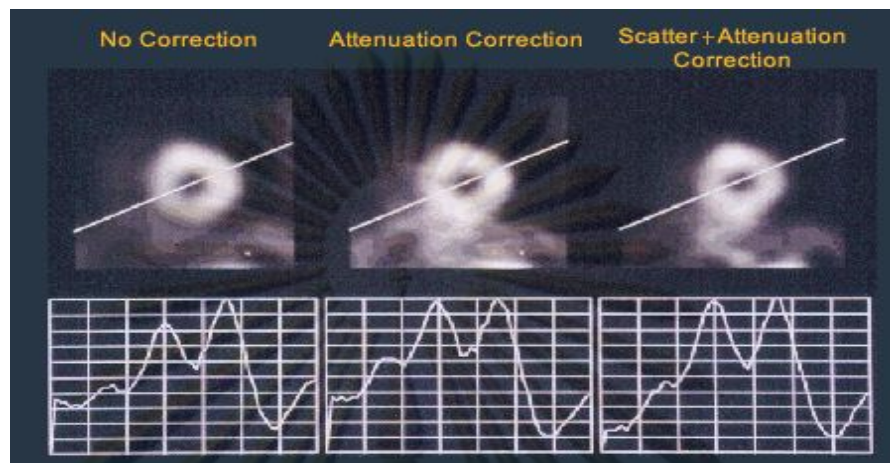


Figure 2.2 : 3 Myocardial perfusion short-axis, left without attenuation correction, middle with attenuation correction, right with scatter and attenuation correction.

2.6 Tomographic Reconstruction [4]

Two common methods of image reconstruction using the acquired data are the filtered backprojection method and iterative method, of which the former is the more popular, although lately the latter is gaining more attention. The filtered backprojection will be described in detail, while the iterative method will be outlined only briefly.

2.6.1 Filtered backprojection [4]

The principle of simple backprojection in image reconstruction, in which three projection views are obtained by a gamma camera at three equidistant angles around an object containing two source of activity designated by black dots. In 360° acquisition, it is a common practice to backproject only the projection of the 180° arc to save computation time, and also the sum or the arithmetic mean of the opposite projection count is taken. In the two-dimensional data acquisition, each pixel count in an image projection represents the sum of all counts along the straight-line path through the depth of the object. Reconstruction is performed by assigning each pixel count of given projection in the acquisition matrix to all pixel along the line of collection in the reconstruction matrix. This is called simple backprojection. Backprojection can be better explained in terms of data acquisition in the computer matrix. Suppose the data are collected in a 4x4 acquisition matrix. In this matrix, each row represents a slice of certain thickness and is backprojected individually. Each row consists of four pixels. More projection views are taken at angles between 0° and 90°, or any other angle greater than 90° and stored in 4x4 acquisition matrices, the all these projections can be similarly backprojected into the reconstruction matrix. This type of backprojection results in superimposition of data in each projection, thereby forming the final transverse image with areas of increased or decreased activity. Using 4x4 matrices, four transverse cross-section images (slice) can be produced. Using 64x64 matrix not different for acquired and reconstruction can be generated 64

transverse slices. All transverse slice, appropriate pixels are sort out the horizontal and ventricle long axis, and to form sagittal and coronal images. That is common practice to lump several slices together to increase the count density in the individual slice to reduce statistic fluctuation. Problem of the simple backprojection are stars-pattern, artifact caused by shinning through radiation from adjacent area of increase radioactivity result in blurring of the object. The blurring effect decreases by apply a filter to acquisition data, and the filtered projection then backprojection to produce an images that the original object. The method call filter backprojection, in general two method of filter backprojection is convolution method in spatial domain and the Fourier method in the frequency domain.

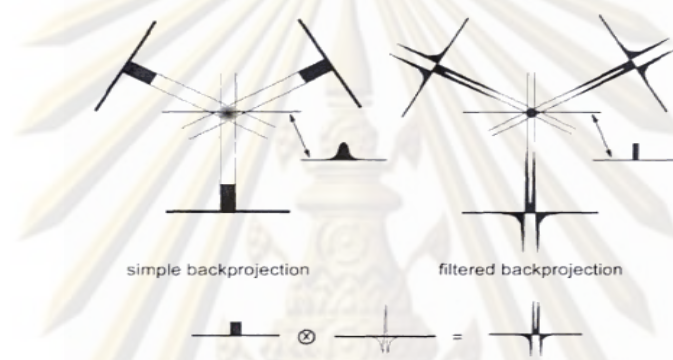


Figure 2.3 Simple backprojection method (left), filtered backprojection method (right).

2.6.1.1 The convolution method [4]

The blurring of reconstruction image cause by filter backprojection is eliminating by the convolution method in kernel, and result data are then backprojection. The application of a kernel is mathematic operations that remove blurring function in term of distance by take some count from the neighboring pixel and put them back into the center pixel of interest. Nine-point smoothing kernel has been widely used in nuclear medicine to decrease statistical variation. This technique is primary to average the count in each pixel with the neighboring pixel in the acquisition matrix. The spatial kernel described above with all positive weighting factors reduce noise but degrade spatial resolution of images. Sharp edges in the original image become blurred in smooth image as result of averaging the count of the edge pixel with the neighboring pixel. Another filter kernel used in spatial domain consists of narrow center peak with both positive and negative values on both side of peak. Edge-sharpening filter is applied central to pixel for correction, the negative value in effect erase all neighboring pixel count density, then created a corrected center pixel value. Repeat for all pixel in each projection and corrected projection are then backprojection. This technique reduces original image with better resolution but increase noise. Blurring due to simple backprojecton is removing by this technique but the noise inherent in the data acquisition due to the limitation of the spatial resolution of image device is not removing but rather enhanced.

2.6.1.2 The Fourier method [4]

Nuclear medicine data obtained in the spatial domain can be expressed in terms of Fourier in the frequency domain as the sum of series of sinusoidal waves of different amplitude, spatial frequency and phase shift run across the image. This is equivalent to sound wave that is composed of many sound frequencies. The data for each row and column of acquisition matrix can be considered as composed of sinusoidal waves of varying amplitude and frequency in the frequency domain. The process of determining the amplitude of a sinusoidal wave is called the Fourier transformation and the method of changing from the frequency domain to the spatial domain is called the inverse Fourier transformation. The Fourier method uses a filter to eliminate the blurring function from the filter backprojection of projection data. The filter does the same thing in image reconstruction, modulating the amplitude of different frequencies while preserving the image represented by low frequencies and removing the noise represented by high frequencies. The results obtained by the Fourier method are identical to those by the convolution method. The Fourier method appears much easier and faster to compute the reconstruction of an image than the convolution method. Nyquist frequency is the Fourier filter that has been designed and used in the reconstruction of images in nuclear medicine and is characterized by its maximum frequency. Nyquist frequency gives an upper limit to the number of frequencies necessary to describe the sine and cosine curves representing an image projection. The maximum number of peaks possible in a projection of acquisition data at the Nyquist frequency is 0.5 cycle/pixel.

2.6.2 Iterative reconstruction [4]

Iterative reconstruction is a method of algorithms used to reconstruct 2D and 3D images from the projections of an object. There are a large variety of algorithms, but each starts with an assumed image, computes projections from the image, compares the original projection data and updates the image based upon the difference between the calculated and the actual projections. Although conceptually this approach is much simpler than filter backprojection, for medical applications it has traditionally lacked the speed of implementation and accuracy. This is due to the slow convergence of the algorithm and high computational demands. The major advantages of the iterative approach include insensitivity to noise and the capability of reconstructing an optimal image in the case of incomplete data. Situations where it is not possible to measure all 180 degrees may be more amenable to solution by this approach. The method has been applied in emission tomography modalities like SPECT and PET.

2.7 Quantitative Analysis [3]

Quantitative methods have been used during the past 10 years to measure cardiac function as well as regional cardiac function from SPECT images. Cardiovascular nuclear medicine techniques are inherently quantitative. This is because the pixel count value from within a cardiac region is related to some parameter of cardiac performance. In the case of myocardial perfusion imaging, the pixel count value from a region is related to the concentration of radionuclide and thus blood flow. Two standard types of quantification are: absolute quantification, which is the ability to extract from a pixel a number of counts expected from a given radionuclide concentration at the source location, and the true relative quantification, which is the ability to extract from pixels the ratio of the counts expected from a given ratio of radionuclide concentrations at two source locations. At the present time, the most

widely used approach has used data-based methods of quantification. The concept of data based quantification involved three major steps:

- a. Image processing to enhance the image.
- b. Image analysis to extract pertinent measurement for use in determining normality versus abnormality.
- c. Comparison of extracted measurement to database of result from normal to qualify the degree abnormality.

Many of the techniques illustrate reflect computer method developed at Cedars-Sinai Medical Center. The Cedars-Sinai quantitative approach to SPECT is based on sampling the patient's short and vertical long axis myocardial tomogram using maximum count circumferential profiles and comparing these profile to profile derived from a database of normal patients. Patient profile points that fall below the normal limit and meet a criterion for abnormality are considered abnormal. The quantitative output of the program includes a polar map display design are abnormality and report indicating the percent of abnormal pixel within the total and individual vascular territories. QPS provides three perfusion polar maps and three 3D parametric surfaces (stress, rest and reversibility). The Function pull-down menu contains the options "Raw", "Severity", and "Extent", all of which apply to both 2D and 3D displays. A grid of 20-segments (Segments), 3 vascular territories (Vessels) or 4 regions (Walls) can be overlaid onto all polar maps and surfaces from the Grid pull-down menu: in the polar maps case, the numbers associated with the overlay represent the average value of the parameter measured by each map within the segment, territory or region in which they lie. Both stress and rest perfusion values are normalized to 100. QPS measurements of the absolute area of perfusion defects can be hampered by incorrect listing of the pixel size in the image. Pixel size is usually automatically calculated based on knowledge of field of view and zoom information.

2.8 Computed Tomography (CT)

2.8.1 Principles of CT [2]

Physically, X-rays can traverse a cross-section of an object along straight lines, attenuated by the object, and detected outside it. During CT scanning, the cross-section is probed with X-rays from various directions; attenuated signals are recorded and converted to projections of the linear attenuation coefficient distribution of the cross-section. These X-ray shadows are directly related to the Fourier transform of the cross-section, and can be processed to reconstruct the cross-section.

The measured attenuations of the X-rays passing through the patient are converted into pixels and CT numbers, measured by Hounsfield units (HU). The 3D CT images are obtained from 2D transverse slices which show anatomical information in terms of tissue densities (HU). Because we cannot see the difference between 2000 different shades of gray it would be pointless to produce an image which covered the whole range of Hounsfield numbers. In order to produce a useful image of the area of interest a system of windowing and levels is used.

The available gray scale is spread over the chosen range of Hounsfield numbers. The window defines the upper and lower limits of this range. To produce an image which shows up most major structures a large window is used. For more

detailed information about tissues with very similar density a small window is used. The smaller the window the more detailed the image but the range of tissue density that is seen is reduced. The level is the Hounsfield number at the centre of the window. This is chosen so that the window covers the type of tissue of interested. To image dense tissues a high level of window setting is used and to image low density tissues a low level window setting is used. Multi-slice detector geometries allow whole-body imaging, reduces scanning times, which the patient discomfort is reduced and movement artifacts in images are minimized. To enhance some structures with similar tissue density values, contrast media are used.

2.8.2 SPECT/CT [7]

A modality which is rapidly evolving from a somewhat under-utilized technical option to gain an acknowledged status for optimizing the diagnostic capabilities of single photon imaging, with potential impact on patient management. SPECT and CT are tomographic imaging procedures, each one with separately proven good diagnostic performance. SPECT produces computer-generated images of local radiotracer uptake, while CT produces 3-D anatomic images of x-ray density of the human body. Combined SPECT/CT imaging provides sequentially functional information from SPECT and the anatomic information from CT, obtained during a single examination. CT data are also used for rapid and optimal attenuation correction of the single photon emission data. By precisely localizing areas of abnormal and/or physiological tracer uptake, SPECT/CT improves sensitivity and specificity, but can also aid in achieving accurate dosimetric estimates as well as in guiding interventional procedures or in better defining the target volume for external beam radiation therapy. Gamma camera imaging with single photon emitting radiotracers represents the majority of procedures in a routine nuclear medicine practice. Many of these examinations are tumors or cardiac imaging studies. The development of better instruments, newer computer based procedures for image analysis and display, new ^{99m}Tc labeled agents for visualizing biologically significant events may enhance the future value of SPECT/CT in terms of both clinical impact on patient care and cost effectiveness, as compared to PET/CT. Diagnosis and characterization of disease by CT imaging is based on morphologic criteria such as size, texture and tissue attenuation. CT provides information regarding changes in organ size and tissue density, as well as their precise spatial localization and topographic landmarks. However, structural data do not necessarily correlate with the metabolic status of disease. On the other hand, nuclear medicine imaging is based on the bio-distribution of a radioactive agent over time and space, thus visualizing dynamic physiological and pathophysiological processes that define the functional characteristics of disease. Furthermore, whole body assessment is possible with a single radiation exposure, as the ionizing agent is administered to patients rather than being delivered from an external source to each region of the body to be evaluated, as performed with radiologic imaging. However, scintigraphic images lack accurate anatomic landmarks for precise localization and characterization of findings, in spite of the fact that specific radiopharmaceuticals are used for assessment and diagnosis of specific disease processes. The above mentioned considerations explain why morphologic and functional imaging modalities are complementary and not competing techniques, especially if precise image registration is made possible by using a single imaging unit combining the emission based data (SPECT) with the transmission based data. Image registration is the process of determining the geometric relationship between

multimodality imaging studies, in order to use information provided by one test in the context of the other modality.

2.9 Review of related literatures

U Daisuke et al. [8] reported research on object-specific attenuation correction at SPECT/CT in thorax. They preliminarily investigated the optimal x-ray tube current for use in attenuation correction. The adequacy of SPECT/CT attenuation coefficient maps was assessed by comparing total counts gamma ray emission from Tl-201 in four regions of interest on the two attenuation corrected images. The size of each region of interest was 5 pixels. To verify the reproducibility of these measurements in phantom, CT at 10 and 140 mA was repeated six times. They compared between high and low current tubes of x-ray, the result found high current provided images quality but increase radiation dose to patient. The data showed no significant difference on count of SPECT.

Preuss R. et al. [9] reported the study on optimization of protocol for low dose CT-derived attenuation correction in myocardial perfusion SPECT imaging. They evaluated the quality of attenuation maps generated with very low tube current to minimize exposure due to transmission scanning. In phantom studies, determination of linear absorption coefficients (μ) for air, water and Teflon was carried out to determine attenuation maps in both stress and resting studies from 62 patients. All patients underwent exercise or pharmacologic stress testing and a resting study for comparison using Tc-99m MIBI or Tc-99m Tetrofosmin. AC in stress studies was performed using 2.5 mA tube current, whereas 1.0 mA was used in resting studies. The result in phantom and patient studies, differences of linear absorption coefficients were not significant. Effective dose in CT-based AC for myocardial perfusion SPECT decreased from 0.90 mSv down to 0.36 mSv (60% reduction) and reliable attenuation maps (μ -maps) of the thorax can be obtained even with the use of very low tube current.

The study by U Daisuke et al. and Preuss R. et al. not study in difference lesion size, vary lesion location and lesion concentration. So our research is designed to study the effect of attenuation correction by varying x-ray tube current-time in phantom of myocardial perfusion SPECT.

ศูนย์วิทยุทรัพยากร

จุฬาลงกรณ์มหาวิทยาลัย

CHAPTER III

RESEARCH METHODOLOGY

3.1 Research design

This research is an experimental, cross-sectional design. The steps of procedures are in figure 3.1.

3.2 Research design model

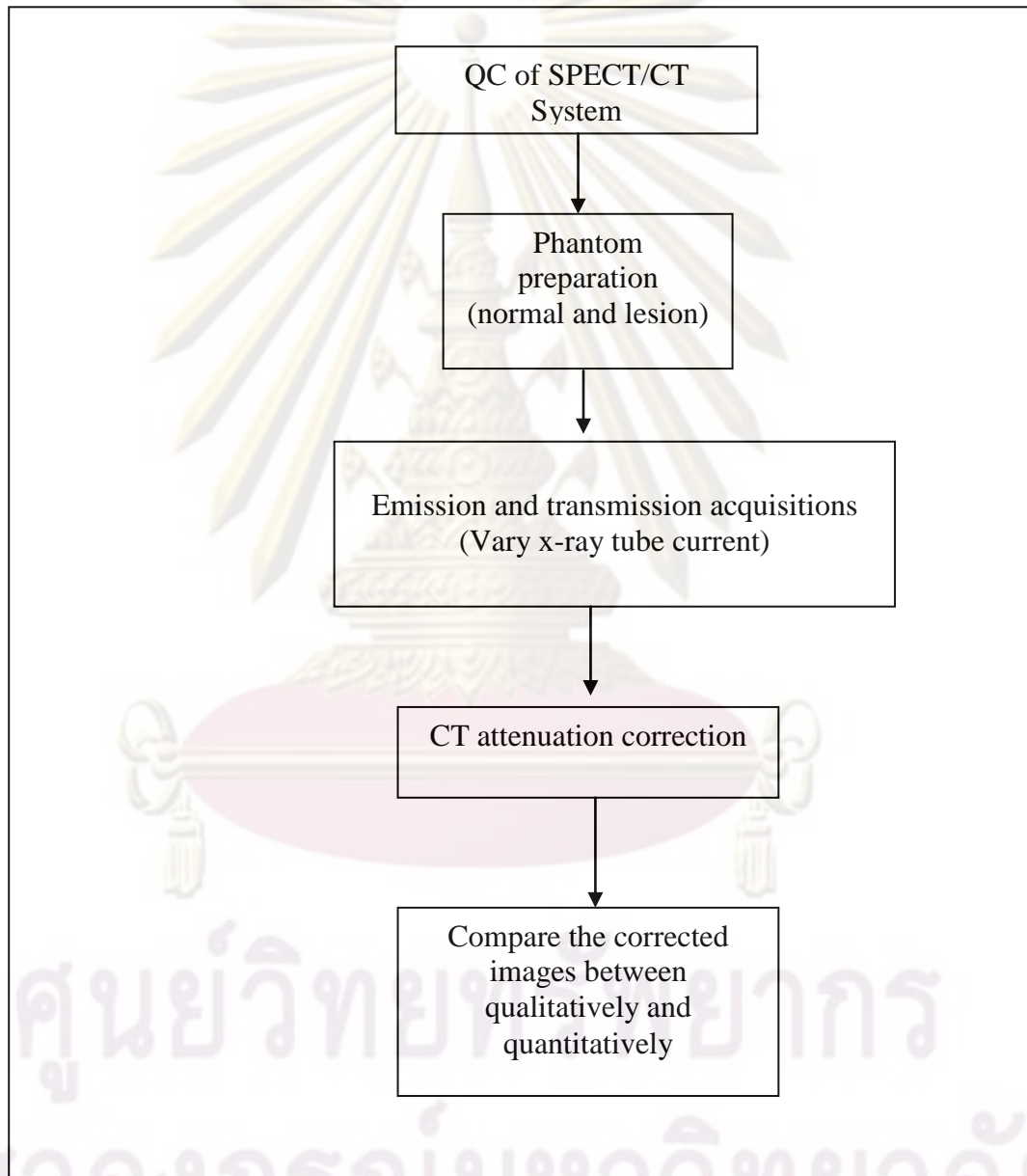


Figure 3.1 Research design model

3.3 Conceptual framework

There are four parameters influencing the image quality from myocardial perfusion SPECT. The line source and CT transmission influences attenuation correction, activity concentration, lesion size and defect location influences of corrected images. The conceptual framework of this study is show in figure 3.2.

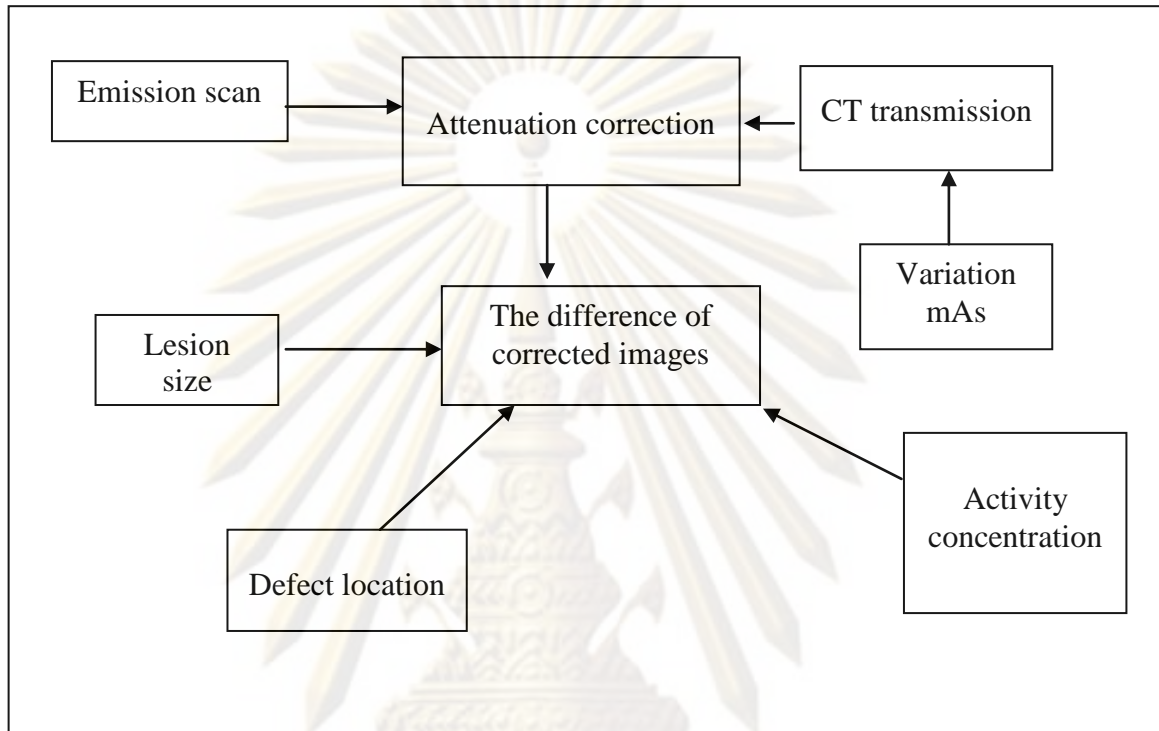


Figure 3.2 Conceptual framework

3.4 Research question

What are the effects of different tube current-time of CT scan on attenuation corrected image obtain from myocardial perfusion SPECT phantom?

3.5 Key words

- Attenuation correction
- Myocardial Perfusion
- SPECT/CT

3.6 The sample

The determination of image uniformity will be studied in normal cardiac phantom without defect insertion using 5 tube current-time of CT scan. Then the determination of defect detectability will be studied in cardiac phantom with defect inserted using 3 tube current-time of CT scan. The inserted defect will be varied into 2 different sizes i.e. 1 x 1.5 and 1 x 2 cm². diameter, 3 different activity concentration i.e. 25%, 50% and 75% of myocardial activity and in 4 different myocardial walls i.e. anterior, inferior, septal, and lateral wall. These will include a total of 231 scans.

3.7 Material

3.7.1 Single Photon Emission Computed Tomography/ Computed Tomography (SPECT/CT)

SPECT/CT system as shows in figure 3.4 is manufactured by Siemens Medical Solution, Model Sembia T6. The system integrates a SPECT scan with 6 multi slice CT scan using Syngo multimodality computer platform. SPECT scan, consist of arrays of NaI(Tl) crystal detector, size is 59.1x44.5 cm, field-of-view (FOV) is 53.3x38.7 cm. and total number of photomultiplier tubes is 59. For CT scan is the able to simultaneously collect data, this 6-row data collection is accomplished via a 6-row detector. The maximum scan FOV is 50 cm. Bore diameter is 70 cm. Three kVp settings are available at 80, 110 and 130 kVp. The tube current ranges from 20 to 345 mA.



Figure 3.4 SPECT/CT

3.7.2 Anthropomorphic SPECT Phantom

Anthropomorphic phantom used in this study include liver, lung, heart and spine insert. Lung inserts filled with Styrofoam beads and water to simulate lung tissue density. Main applications to evaluation of cardiac ECT data acquisition and reconstruction with non-uniform attenuation correction methods. The cardiac insert with the following dimension is chamber length 8.6 cm, diameter 6 cm and myocardial volume ~ 110 cc and ventricle volume ~ 60 cc. The volumes are left lung 0.9 liters, right lung 1.1 liter, liver 1.2 liters and background 10.3 liters.



Figure 3.5 (left) ventricle chamber (right) myocardium chamber.

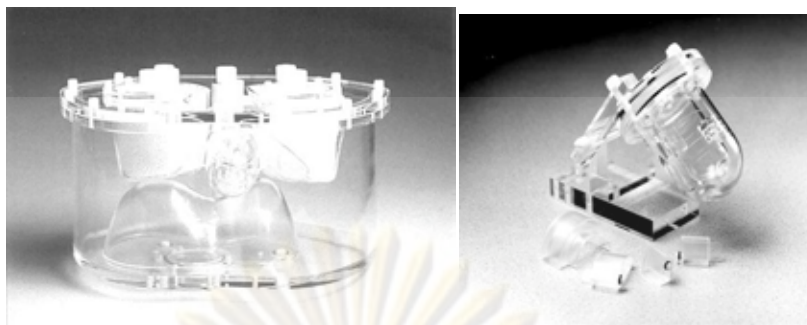


Figure 3.6 Anthropomorphic SPECT Phantoms

3.8.3 Technetium pertechnetate ($^{99m}\text{TcO}_4^-$)

Technetium-99m is a metastable nuclear isomer of technetium-99, symbolized as ^{99m}Tc . The "m" indicates that this is a metastable nuclear isomer, i.e., that its half life is considerably longer than most nuclear isomers which undergo gamma decay. As in all gamma decay reactions, a metastable nuclear isomer does not change into another element upon its isomeric transition or "decay". The life-time of technetium-99m is very long in terms of average gamma-decay half-lives, though short in comparison with half-lives for other kinds of radioactive decay, and in comparison with radionuclide used in many kinds of nuclear medicine tests. Technetium-99m is used as a radioactive tracer detected in the body. It is well suited to the role because it emits readily detectable 140 keV gamma rays and its half-life for gamma emission is 6.0058 hours. The short half life of the isotope allows for scanning procedures which collect data rapidly, but keep total patient radiation exposure low. In the myocardial perfusion scans using Tc-99m, the radiopharmaceuticals ^{99m}Tc -tetrofosmin or ^{99m}Tc -sestamibi are used. Scanning may then be performed with a conventional gamma camera, or with SPECT. This study perform in a phantom so used $^{99m}\text{TcO}_4^-$ because low cost and mechanism similar as ^{99m}Tc -tetrofosmin or ^{99m}Tc -sestamibi.

3.9 Methods

This study is carried out as the following:

3.9.1 SPECT/CT daily QC [APPENDIX C]

The daily quality control program for CT and SPECT is regularly performed using water phantom for the study of CT image quality, kVp calibration, pixel noise and CT number values. The flood-field uniformity can be evaluated intrinsic, the former represent baseline response of the detector operation. Uniformity is measured over the useful field of view and central filed of view, frequency of test is daily. The COR must be accurately aligned with the center of the acquisition matrix in the computer, frequency of test is weekly.

3.9.2 Phantom preparation

The outer myocardial wall fills with Tc-99m activity 700 $\mu\text{Ci}/110$ cc. The ventricle chamber fills with Tc-99m activity 73 $\mu\text{Ci}/61$ cc. Background of the phantom fills with Tc-99m activity 0.1 $\mu\text{Ci}/\text{cc}$ with the total background volume of

10,300 ml. The inserted lung not filled Tc-99m activity and liver filled with Tc-99m activity 0.2 $\mu\text{Ci}/\text{cc}$ with the volume of 1,200 cc. The solution is well mixed before filling into the phantom.

The activity concentration, which is filled into the inserted myocardial defect, will be varied into 3 different concentrations i.e. 25%, 50% and 75% of the normal outer myocardial wall concentration.



Figure 3.7 lesion size 1x1.5 and 1x2 cm^2

3.9.3 SPECT/CT procedure

The acquisitions protocol consists of 32 projections for 30 seconds over 180-degree arc extending from 45 degree RAO to 45 degree LPO projection. The simplest automatic contour consists of approximating the object outline by an ellipse drawn around the edges of the object. Uniform attenuation is then assigned within the contour to generate the attenuation map. Standard protocols of emission scan of step and shoot, 3 degree per step, matrix size 64x64 Zoom 1.45 were used. For CT scan, the parameters such as tube voltage (kVp), collimation, slice width, and pitch factor were fixed as in table 3.1. The acquisition time for the chest scan is about 5 minutes. The projection data for each phantom were generated with two techniques of reconstruction as follows:

Filterback projection (FBP) images: the data was reconstructed by Butterworth filter nyquist frequency 0.45 power 5 smooth kernel B08s to smooth images without attenuation.

An iterative reconstruction image was applied for attenuation by order 8 and subset 8. The quantitative perfusion SPECT (QPS) algorithms represent mean count/pixel for all segments, as well as the polar map (bull's eye). Bull's eye from QPS program is displayed to evaluate quantity of myocardial perfusion images. The picture shows % perfusion in each wall of myocardium in term of normalized count per pixel.

Table 3.1 CT scan parameters for mediastinum SPECT/CT scan.

Collimation (mm)	Slice width (mm)	FOV(mm)	Pith factor
6x3	5	500	0.6

3.9.4 Data collection

To determine the uniformity of the attenuation correction process of each tube current-time of CT scan, the data from left ventricular wall of myocardial phantom without defect-inserted are used. The left ventricular wall is divided into 4 regions which are anterior, septal, inferior and lateral walls. The percent normalized value of the average attenuation corrected counts of each region is calculated as shown in equation 3.1[11]. The percent normalize value defines uniformity index, ideally it should be 100%. Five tube current-time of CT scan, i.e. mAs 34, 43-48, 100, 150 and 200, used to determine the percent normalized value. The tube current-time of 43-48 is the Automatic Exposure Control (AEC) mode. It is designed by the SPECT manufacturer to try to reduce radiation exposure to the patient.

$$\% \textit{normalization value} = \frac{\textit{count per pixel of each region}}{\textit{maximum count per pixel of 4 region}} \times 100 \quad (3.1)$$

To determine the lesion detectability, percentage contrast of lesion is calculated using equation as shown in equation 3.2. [11] The higher the percent contrast of the lesion, the better ability to detect the lesion. Again the percentage contrast of lesion is calculated for the lesion in each of the 4 walls separately. The percent contrast of lesion is studied using only 3 different tube current-time of CT scan only which are mAs 34, 43-48 and 200. This study selected 3 tube current-time set as default by the manufacturer, due to constraints of the manufacturer, the lowest tube current available was 34 mAs, routine clinical used as AEC mode and routine clinical used in radiology diagnosis technique.

$$\% \textit{Contrast of lesion} = \left| \frac{C_{\textit{lesion}} - C_{\textit{uniform}}}{C_{\textit{uniform}}} \right| \times 100 \quad (3.2)$$

Where $C_{\textit{lesion}}$ is the average count per pixel in the region where defect is inserted and $C_{\textit{uniform}}$ is the average count per pixel in the other 3 myocardial regions where no defect is inserted.

3.10 Statistical analysis

Data are expressed as mean \pm SD. Comparison of the percent normalized value and percentage contrast of lesion between lesions locations, lesion size, lesion concentration in different tube current-time are performed using pair t –test. A p value of less than 0.05 is considered statistically significant.

3.11 Ethical Consideration

This study is performed in myocardial perfusion SPECT phantom. The ethical is accepted by Ethics Committee of Faculty of Medicine, Chulalongkorn University.

3.12 Expected Benefits

The effects of different tube-current time in attenuation correction process of myocardial perfusion study, i.e. uniformity of the image, the detectability of different defect size, location and activity concentration, will be obtained.

The optimal tube-current time of CT scan for the patient study to obtain the optimal image quality while expose the minimum radiation dose to the patient.

CHAPTER IV

RESULTS

4.1. The percent normalized value

The percent normalized values of each wall of myocardial phantom without defect inserted using various tube current-time, 3 scans for each mAs are shown in table 4.1 and figure 4.1

Table 4.1 The percent normalized values of each wall of myocardial phantom without defect.

Tube current-time (mAs)	Percent normalization value in each wall			
	Anterior wall	Inferior wall	Lateral wall	Septal wall
34	98.63	92.93	89.56	91.65
	93.82	93.25	94.78	94.22
	100.00	92.05	89.64	93.49
AEC (43-48)	95.39	100.00	99.18	95.96
	98.68	99.92	99.01	95.63
	99.75	99.84	99.92	94.98
100	99.11	92.17	95.24	93.95
	100.00	92.82	95.32	92.66
	99.03	92.90	95.24	92.57
150	94.78	95.10	92.65	92.16
	99.27	94.61	92.73	98.45
	100.00	95.27	92.57	92.08
200	99.68	93.45	96.40	94.08
	100.00	93.29	96.80	100.00
	99.92	93.37	96.88	95.68

Table 4.2 The p-values of the paired t-test statistics comparison of the percent normalized values of each wall of myocardial phantom without defect inserted.

Parameter compare (mAs)	p-value			
	34	AEC	100	150
AEC	0.028*	-	-	-
100	0.113	0.897	-	-
150	0.12	0.005*	0.897	-
200	0.0034*	0.190	0.02*	0.041*

*two-tailed p-value statistically significant.

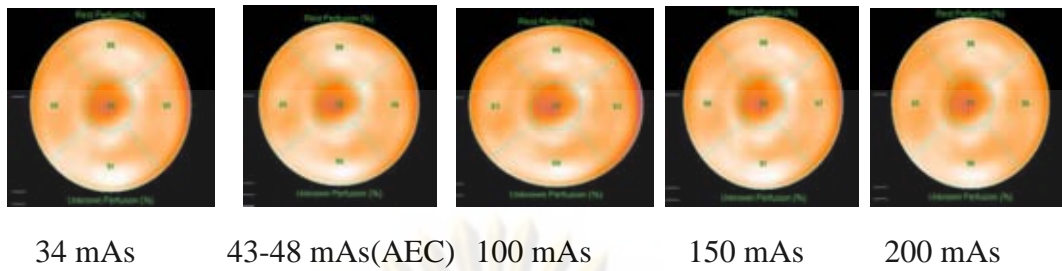


Figure 4.1 Bull's eye map of defect free phantom in different tube current-time

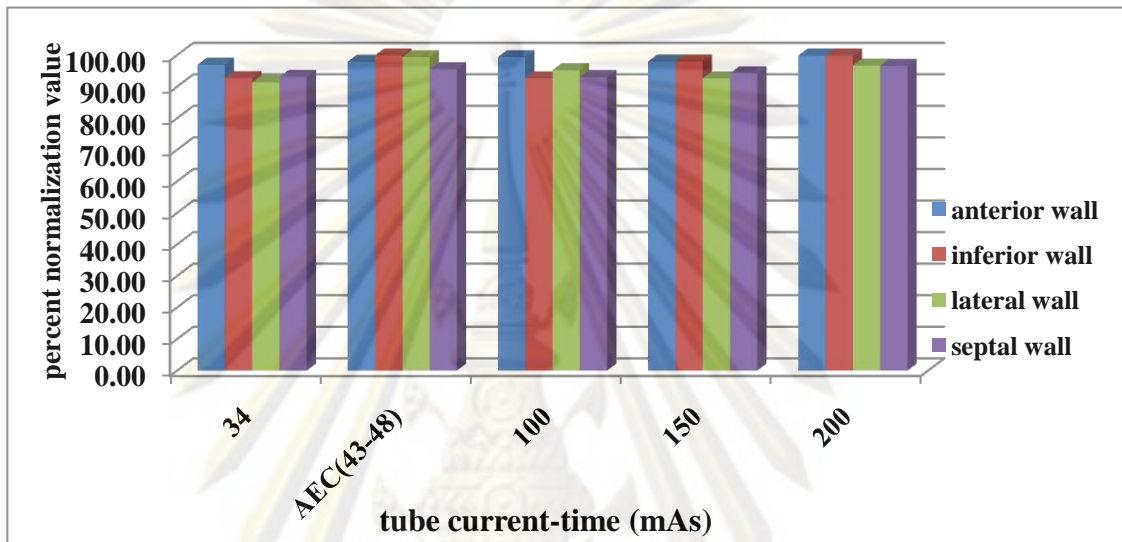


Figure 4.2 The percent normalize values in 4 myocardial walls using different tube current-time

4.2. The percentage contrast of lesion

The percent contrasts of lesion of each wall of myocardial phantom with variation of inserted defect using 3 different tube current-times are shown in table 4.3 and figure

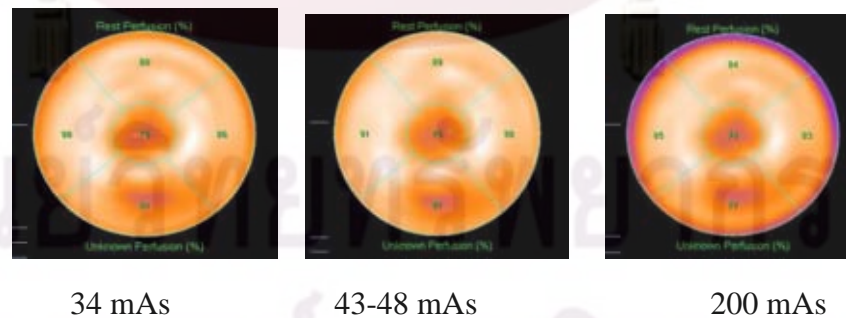


Figure 4.3 Bull's eye map of lesion size 1x1.5 cm², 75% lesion concentration and lesion at inferior wall on 34, 43-48 and 200 mAs respectively.

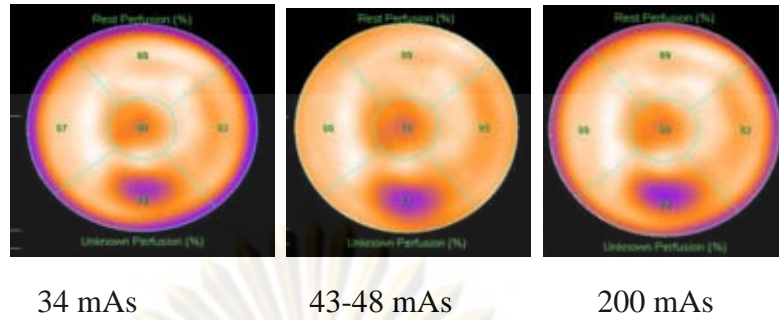


Figure 4.4 Bull's eye maps of lesion size $1 \times 1.5 \text{ cm}^2$, 50% lesion concentration and lesion at inferior wall on 34, 43-48 and 200 mAs respectively.

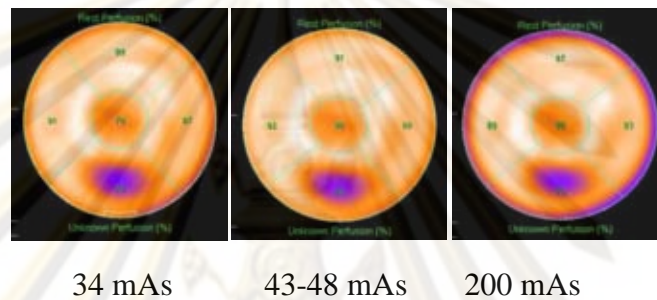
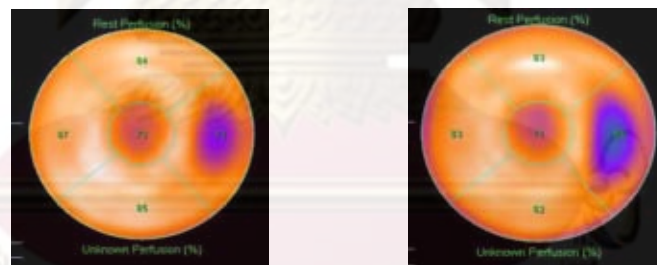


Figure 4.5 Bull's eye map of lesion size $1 \times 1.5 \text{ cm}^2$, 25% lesion concentration and lesion at inferior wall on 34, 43-48 and 200 mAs respectively.



(Left) Lesion size $1 \times 1.5 \text{ cm}^2$ (Right) Lesion size $1 \times 2 \text{ cm}^2$

Figure 4.6 Bull's eye maps of lesion size $1 \times 1.5 \text{ cm}^2$ and $1 \times 2 \text{ cm}^2$ lesion at lateral wall

ศูนย์วิทยุทรัพยากร
จุฬาลงกรณ์มหาวิทยาลัย

Table 4.3 The percent contrasts of lesion of each wall of myocardial phantom with variation of inserted variation defect using 3 different tube current-times, 3 scans. (Lesion size 1x1.5cm²)

Lesion size (cm)	Lesion concentration	Lesion location	% contrast of lesion		
			mAs 34	mAs 43-48	mAs 200
1x1.5	25%	Anterior	77.88	77.94	79.26
			79.13	79.41	78.80
			78.77	78.09	79.20
1x1.5	25%	Inferior	75.68	77.75	76.02
			76.46	78.51	75.82
			76.44	76.39	76.04
1x1.5	25%	Lateral	78.40	79.73	79.61
			79.29	79.89	80.48
			80.07	80.10	79.65
1x1.5	25%	Septal	74.54	76.75	77.62
			75.37	77.51	77.95
			75.34	76.39	78.61
1x1.5	50%	Anterior	47.58	45.51	44.53
			47.58	43.42	45.60
			47.03	45.36	43.29
1x1.5	50%	Inferior	46.58	44.51	42.53
			45.58	41.42	44.60
			46.03	45.36	42.29
1x1.5	50%	Lateral	54.92	52.21	49.54
			56.20	53.64	52.06
			57.07	53.64	52.06
1x1.5	50%	Septal	52.21	54.71	58.92
			53.64	58.58	58.20
			53.64	58.00	59.07
1x1.5	75%	Anterior	33.36	33.21	38.16
			38.66	35.52	37.71
			34.99	35.52	38.16
1x1.5	75%	Inferior	29.78	28.06	34.52
			33.07	28.87	34.52
			38.36	28.06	32.38
1x1.5	75%	Lateral	30.81	30.98	32.81
			32.94	31.58	31.94
			30.66	30.98	32.66
1x1.5	75%	Septal	28.81	32.21	32.89
			32.94	32.58	30.87
			29.66	31.98	30.87

Table 4.4 The percent contrasts of lesion of each wall of myocardial phantom with variation of inserted variation defect using 3 different tube current-times and 3 scans. (Lesion size 1x2cm²)

Lesion size (cm)	Lesion concentration	Lesion location	% contrast of lesion		
			mAs 34	mAs 43-48	mAs 200
1x2	25%	Anterior	78.11	79.62	80.17
			78.39	79.65	79.79
			79.97	81.22	79.76
1x2	25%	Inferior	77.75	78.25	78.46
			78.08	78.12	77.19
			78.10	78.62	78.17
1x2	25%	Lateral	80.10	81.62	81.17
			79.58	80.65	80.79
			79.55	81.22	79.76
1x2	25%	Septal	77.75	78.25	78.46
			78.08	79.12	77.19
			78.06	78.59	78.46
1x2	50%	Anterior	54.37	55.48	58.33
			56.30	54.90	58.64
			55.24	54.41	57.69
1x2	50%	Inferior	48.07	47.09	51.79
			48.46	46.60	51.40
			47.51	47.02	50.37
1x2	50%	Lateral	52.37	56.48	59.33
			57.30	54.90	57.64
			55.24	55.41	58.69
1x2	50%	Septal	46.07	48.09	50.79
			48.46	46.60	50.40
			47.51	48.02	51.37
1x2	75%	Anterior	22.39	25.08	26.83
			25.58	24.28	29.23
			26.86	29.45	26.83
1x2	75%	Inferior	26.09	26.68	28.02
			26.09	27.21	29.93
			26.09	27.21	27.92
1x2	75%	Lateral	33.50	30.02	37.10
			30.67	30.09	38.64
			30.26	30.02	37.78
1x2	75%	Septal	27.09	28.68	29.02
			26.09	28.21	28.93
			28.09	27.28	28.92

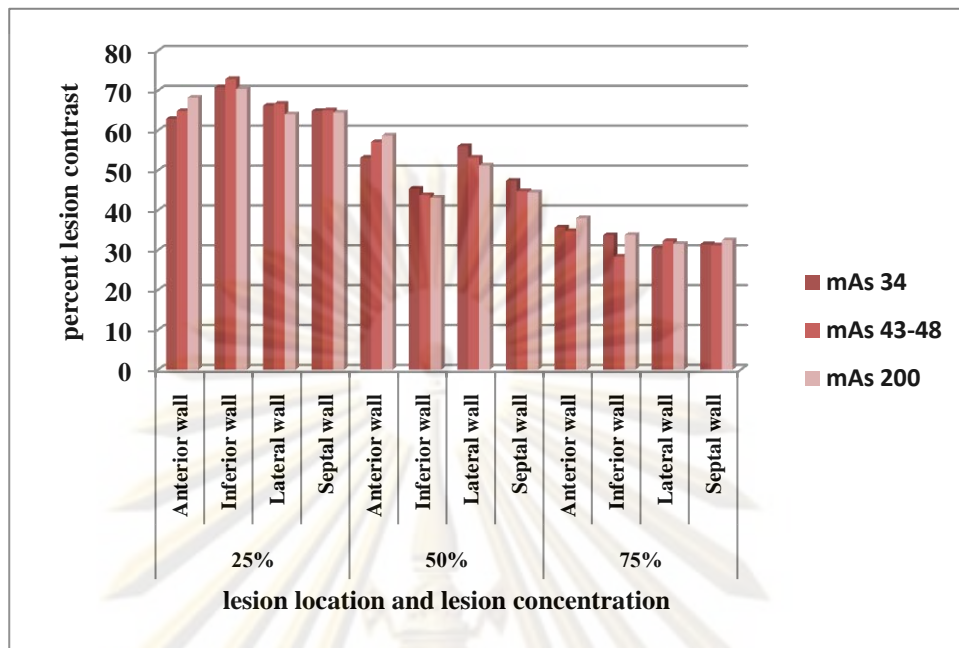


Figure 4.7 The percent contrast of lesion size 1 x 1.5 cm². with various tube current-times in different wall and different activity concentration.

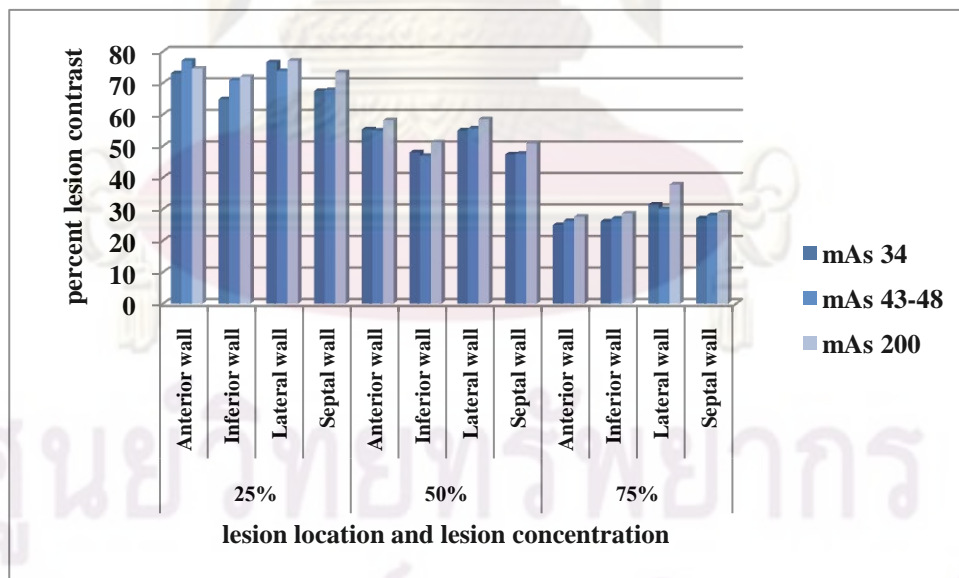


Figure 4.8 The percent contrast of lesion size 1 x 2 cm². with various tube current-times in different wall and different activity concentration.

The percent contrast of different lesion parameters using different tube current-time are compared using t-test and the p-values are shown in table 4.5-4.11

Table 4.5 The p-values of the paired t-test statistics comparison of the percent contrast of different lesion parameters using different tube current-time, at 25% lesion concentration of myocardium and lesion size 1x1.5 cm²

Parameter compared (lesion location)	Lesion concentration	p-value		
		mAs 34	mAs 43-48	mAs 200
Anterior and Inferior	25	0.003*	0.17	0.006*
Anterior and Lateral		0.18	0.09	0.19
Anterior and Septal		0.0013*	0.17	0.08
Inferior and Lateral		0.0002*	0.18	0.01*
Inferior and Septal		0.008*	0.07	0.007*
Lateral and Septal		0.0045*	0.015*	0.051

* two-tailed p-value statistically significant.

Table 4.6 The p-values of the paired t-test statistics comparison of the percent contrast of different lesion parameters using different tube current-time, at 50% lesion concentration of myocardium and lesion size 1x1.5 cm²

Parameter compared (lesion location)	Lesion concentration	p-value		
		mAs 34	mAs 43-48	mAs 200
Anterior and Inferior	50	0.057	0.22	0.057
Anterior and Lateral		0.008*	0.01*	0.02*
Anterior and Septal		0.01*	0.019*	0.004*
Inferior and Lateral		0.007*	0.02*	0.01*
Inferior and Septal		0.01*	0.02*	0.004*
Lateral and Septal		0.008*	0.03*	0.01*

* two-tailed p-value statistically significant.

Table 4.7 The p-values of the paired t-test statistics comparison of the percent contrast of different lesion parameters using different tube current-time at 75% lesion concentration of myocardium and lesion size 1x1.5 cm²

Parameter compared (lesion location)	Lesion concentration	p-value		
		mAs 34	mAs 43-48	mAs 200
Anterior and Inferior	75	0.55	0.01*	0.03*
Anterior and Lateral		0.044*	0.03*	0.005*
Anterior and Septal		0.004*	0.08	0.008*
Inferior and Lateral		0.49	0.0006*	0.25
Inferior and Septal		0.35	0.0001*	0.08
Lateral and Septal		0.22	0.005*	0.23

* two-tailed p-value statistically significant.

Table 4.8 The p-values of the paired t-test statistics comparison of the percent contrast of different lesion parameters using different tube current-time, at 25% lesion concentration of myocardium and lesion size 1x2 cm²

Parameter compared (lesion location)	Lesion concentration	p-value		
		mAs 34	mAs 43-48	mAs 200
Anterior and Inferior	25 %	0.23	0.04*	0.02*
Anterior and Lateral		0.32	0.22	0.18
Anterior and Septal		0.24	0.13	0.03*
Inferior and Lateral		0.02*	0.008*	0.04*
Inferior and Septal		0.42	0.44	0.42
Lateral and Septal		0.02*	0.04*	0.06

* two-tailed p-value statistically significant

Table 4.9 The p-values of the paired t-test statistics comparison of the percent contrast of different lesion parameters using different tube current-time at 75% lesion concentration of myocardium and lesion size 1x2 cm²

Parameter compared (lesion location)	Lesion concentration	p-value		
		mAs 34	mAs 43-48	mAs 200
Anterior and Inferior	50 %	0.004*	0.0016*	0.0012*
Anterior and Lateral		0.74	0.18	0.66
Anterior and Septal		0.0005*	0.0056*	0.005*
Inferior and Lateral		0.03*	0.0016*	0.006*
Inferior and Septal		0.42	0.18	0.66
Lateral and Septal		0.009*	0.0016*	0.003*

* two-tailed p-value statistically significant

Table 4.10 The p-values of the paired t-test statistics comparison of the percent contrast of different lesion parameters using different tube current-time at 75% lesion concentration of myocardium and lesion size 1x2 cm²

Parameter compared (lesion location)	Lesion concentration	p-value		
		mAs 34	mAs 43-48	mAs 200
Anterior and Inferior	75 %	0.47	0.67	0.02*
Anterior and Lateral		0.10	0.14	0.0019*
Anterior and Septal		0.23	0.46	0.24
Inferior and Lateral		0.03*	0.003*	0.0013*
Inferior and Septal		0.22	0.23	0.66
Lateral and Septal		0.07	0.03*	0.0028*

* two-tailed p-value statistically significant

Table 4.11 The p-values of the paired t-test statistics comparison of the percent contrast of different lesion size using different tube current-time and lesion concentration.

Parameter compared : Lesion size 1.5 and 2 cm	p-value		
	34 mAs	43-48 mAs (AEC)	200 mAs
25 % lesion concentration	0.004*	0.001*	0.008*
50 % lesion concentration	0.63	0.49	0.051
75 % lesion concentration	0.003*	0.0023*	0.009*

*two-tailed p-value statistically significant.



ศูนย์วิทยทรัพยากร
จุฬาลงกรณ์มหาวิทยาลัย

CHAPTER V

DISCUSSION AND CONCLUSION

5.1 Discussions

5.1.1 Percent normalize

The uniformity of the images as determined by percent normalize value shows that images acquired by higher tube current-time, i.e. mAs 43-48, 100, 150 and 200, do not significantly differ but significantly better than those acquired by the low tube-current time of mAs 34. For example $p \leq 0.028$ for mAs 34 as compare with mAs 43-48, while $p \leq 0.19$ for mAs 43-48 compare with mAs 200. This is in consistent with the study by Kalra MK et al. who optimized the radiation exposure by varying the CT parameter technique and found that the low tube current produce high noise images representing poor quality, while high tube current decreased image noise and gave good image quality but resulted in higher radiation dose than the low tube current.[12] Our results suggest that the tube-current time of mAs 43-48 which is used in AEC mode is a preferably parameter for routine used because it gives good image quality while provides low radiation dose to patient.

5.1.2 Percent contrast of lesion

The comparison results of the percent contrast of 2 lesion sizes show no significant difference using any value of tube current-time of CT scan. This is likely because there is only a small difference of lesion size (0.5 cm difference) so that it does not effect the average count of the region where defect presents. Concerning the difference between defect activity concentrations, as we can expect, there is significant difference of the percent contrast of lesion using activity concentration between 25% and 75% for all value of tube current-time of CT scan. There are no difference when compared 25% with 50% and 50% with 75%, because there is small difference of the activity concentration.

Concerning the results comparison of the percent contrast of lesion in various myocardial locations and various tube current-times of CT scan, the results show non-uniform pattern of p -value. Some pairs of data show significant difference while others show no significant difference. And they are not be able to explain by any reason. For example, the significant difference would be expected between the lesion in lateral wall and septum because of the difference of distance of each myocardial wall from the chest wall. But our results show no significant difference no matter what value of the tube current-time used, while there is significant difference between lesion in inferior and septal wall using mAs 34 but not mAs 200. The uncertainties due to the technical error of phantom preparation. However, the inconsistent results may mean that there is likely that no matter what tube current-time is used there may be no effect on lesion detectability. And until a better method will be discovered, the CT-based attenuation correction is still the preferable choice for transmission scanning. [13] Even through this study did not report the lesion size and lesion concentration. Another study by Nakpoonabutr W et al. showed that quantitative scatter attenuation resolution recovery (QuaSAR) correction methods improved percent of lesion contrast in various locations of myocardium when compare with FBP. Resolution recovery can also be included in iterative reconstruction and iterative filter backprojection methods. [13].

5.2 Conclusion

This study reveals the effect of attenuation correction of myocardial perfusion SPECT images by varying the tube current-time of CT in myocardial phantom studies. The study indicated that any tube current-time of CT-base attenuation correction has no significant effect on percent lesion contrast at percent lesion activity more closely to myocardium activity. However on the clinical practice, this effect should be observed. Although the low tube current-time can reduce radiation dose to the patient, inversely the high tube current-time will increase the patient dose. So, the middle ranges of tube-current-time at 43-48 mAs or AEC mode, which is the compromise technique, according to the ALARA principle should be selected.

This technique not only provides comparable attenuation correction with tube current-time at 200 mAs, but also preserved the image quality and the radiation dose to the patient.



ศูนย์วิทยทรัพยากร
จุฬาลงกรณ์มหาวิทยาลัย

REFERENCES

- [1] Gordon E D, Garcia E V G, Berman D S. Cardiac SPECT imaging (second edition).2000:3-100.
- [2] James A P and Timothy G T. SPECT/CT Physical Principles and Attenuation Correction. Journal Nuclear Medicine Technology. 36(2008): 1-10.
- [3] Health Physics Society. Radiation term and definitions. [Online]. Available from: <http://hps.org/publicinformation/radterms>.
- [4] Saha G B. Physics and Radiobiology of Nuclear Medicine (second edition).2000: 141-164.
- [5] Dominique D, Coleman Edward R, Milton J G. Procedure Guideline for SPECT/CT imaging. J Nuc Med. 47(2006):1227-1234.
- [6] Enviar C, Correction for Attenuation Scatter in SPECT. [Online]. Available from:<http://www2.alasbimnjournal.cl/alasbimn/CDA/imprime/0,1208,PRT%253D454,00.html>. [2002, Oct].
- [7] Mettler F. and Guiberteau M. Instrumaton. Essentials of Nuclear Medicine Imaging. Fifth Edition. Philadelphia Pennsylvania: Saunders Elsevier, 2006.
- [8] Utsunomiya D, Nakaura T, Honda T, Shiraishi S, Tomiguchi S, Morishita S, Awai K, Ogawa H, Yamashita Y. Object-specific attenuation correction at SPECT/CT in Thorax: Optimazation of respiratory Protocol for Image Registration. J Radiology. 237(2005):662-669.
- [9] Preuss R, Weise R, Lindner O, Fricke E, Fricke H, Burchert W. Optimisation of protocol for low dose CT-derived attenuation correction in myocardial perfusion SPECT imaging. European Journal of Nuclear medicine and Molecule Imaging. 35(2008):1133-1141.
- [10] Gopal B S. Production of radionuclide. Physics and Radiobiology of Nuclear Medicine (second edition).2000: 40-50.
- [11] Rosenthal MS, Cullom J, Hawkin W, Moore SC, Tsui BB, Yester M. Quantitative SPECT imaging: A Review and Recommendations by the Focus Committee of the Society of Nuclear Medicine Computer and Instrumentation Concil. J Nuc Med. 36(1995):1489-1513.
- [12] Kalra MK, Maher MM, Toth TL, Hamberg LM, Blake MA, Shepard JA and Saini S. Strategies for CT Radiation Dose Optimization. J Radiology. 230(2004): 619-628.

- [13] Souvatzoglou M, Bengel F, Busch R, Kruschke C, Fernolendt H, Lee D, Schwaiger M, and Nekolla NG. Attenuation correction in cardiac PET/CT with three different CT protocols: a comparison with conventional PET. Eur J Nucl Med Mol Imaging .34(2007):1991–2000.
- [14] Nakpoonabutr W, Krisanachinda A, Pasawang P and Sontarapornpoln T. Optimum correction techniques in myocardial SPECT imaging. MSc.Thesis Mahidol University . (2007): 51-54.



ศูนย์วิทยทรัพยากร
จุฬาลงกรณ์มหาวิทยาลัย



APPENDICES

ศูนย์วิทยทรัพยากร
จุฬาลงกรณ์มหาวิทยาลัย

APPENDIX A

Case Record Form Examinations

Data record form

Date

Current Tube

Radionuclide activity (Tc-99m).....time

Lesion size	Lesion concentration	Lesion location	Average count per pixel			
			Anterior	Inferior	Lateral	Septal
Normal	Normal	-				
1x1.5	25%	Anterior				
1x1.5	25%	Inferior				
1x1.5	25%	Lateral				
1x1.5	25%	Septal				
1x1.5	50%	Anterior				
1x1.5	50%	Inferior				
1x1.5	50%	Lateral				
1x1.5	50%	Septal				
1x1.5	75%	Anterior				
1x1.5	75%	Inferior				
1x1.5	75%	Lateral				
1x1.5	75%	Septal				
1x2	25%	Anterior				
1x2	25%	Inferior				
1x2	25%	Lateral				
1x2	25%	Septal				
1x2	50%	Anterior				
1x2	50%	Inferior				
1x2	50%	Lateral				
1x2	50%	Septal				
1x2	75%	Anterior				
1x2	75%	Inferior				
1x2	75%	Lateral				
1x2	75%	Septal				

จุฬาลงกรณ์มหาวิทยาลัย

APPENDIX B

NEMA Standards Publication NU 2-2001

Performance Measurements of Single Photon Emission Tomographs

SPECT Phantom for test performance characteristic of SPECT scans

The requirement of NEMA for test performance characteristic of SPECT scan was introduced SPECT phantom set, consist of torso phantom IEC/2001, and scatter phantom and sensitivity phantom.

1. Total performance phantom

The phantom as show in figure I, is an International Electric Commission (IEC) body phantom set, used for evaluated image quality in SPECT scan, which consists of a Jaszczak cavity, and 6 fillable spheres with inner diameter of 9.5, 12.7, 15.9, 19.1, 25.4 and 31.8 mm and wall thickness of 1 mm.



Figure I. Jaszczak phantom

Rods size detection 4 group from 6 groups.

Comment: Attenuation coefficient increase to produced image resolution decrease.

Quality Control of SPECT/CT, Part of CT

1. Alignment of Table to Gantry

Method

Locate the table midline using a ruler and mark it on a tape affixed to the table. With the gantry untitled, extend the table top into gantry to tape position. Measure the horizontal deviation between the gantry aperture centre and the table midline. The Deviation should be within 5 mm.

Results:

	Table(cm)	Bore(cm)
Distance from Right to Centre (mm):	20	35
Distance from Centre to Left (mm):	20	35
Measured Deviation (mm):	0	0

Comment: Pass

2. Table Increment Accuracy

Method

Tape a measuring tape at the foot end of the table. Place a paper clip at the center of the tape to function as an indicator. Load the table uniformly with 150 lbs. From the initial position move the table 300, 400 and 500 mm into the gantry under software control (+ ve). Record the relative displacement of the pointer on the ruler. Reverse the direction of motion (-ve) and repeat. Repeat the measurements four times.

Results:

Indicated	Measured	Deviation
300	300	0
400	400	0
500	500	0
-300	-300	0
-400	-400	0
-500	-500	0

Comment: Pass

3. Slice Increment Accuracy

Method

Set up as you would for beam profile measurement. Select 110 Kvp, 100 mAs, smallest slit width. Perform several scans with different programmed slice separations under auto control. Scan the film with a densitometer and measure the distance between the peaks.

Result:

Slice Sep in mm	Measured Sep in mm	Deviation
20	20	0
30	30	0
50	50	0

Comment: Pass

4. Slice Thickness Accuracy

Method

Set up as you would for beam profile measurement. Select 110 Kvp, 100 mAs, smallest slit width. Perform several scans with different programmed slice thicknesses under auto control. Scan the film with a densitometer and measure the full width at half maximum distance.

Result:

Slice Thick in mm	Measured Thick in mm	Deviation
1	1	0
3	3	0
5	5	0
10	10	0

Comment: Pass

5. Position Dependence and S/N Ratio of C.T. Numbers

Method

Position the C.T. head phantom centered in the gantry. Using 1 cm slice thickness, obtain one scan using typical head technique. Select a circular region of interest of approximately 400 sq. mm. And record the mean C.T. number and standard deviation for each of the positions 1 through 5.

Technique:

Kvp	130	mA	250	Seconds	1
-----	-----	----	-----	---------	---

Results:

Position	Mean C.T. #	S.D.	C.V.
1	13.3	2.1	0.158
2	13.6	2.2	0.162
3	13.7	2.3	0.168
4	13.4	2.2	0.164
5	13.8	2.5	0.181

Comment: Pass

6. High Contrast Resolution

Method

Set up the mini C.T. performance phantom as described in beam alignment. Select the section containing the high resolution test objects. Select the head technique. Perform a single transverse scan. Select the area containing the high resolution test objects and zoom as necessary. Select appropriate window and level for the best visualization of the test objects. Record the smallest test object visualized on display monitor.

Technique:

Kvp	130	mA	250	Seconds	1
-----	-----	----	-----	---------	---

Result:

Slice Thickness in mm	Resolution
1	15 lp/cm
2	15 lp/cm
3	15 lp/cm
5	17 lp/cm
10	17 lp/cm

Comment: Pass

7. Low contrast Resolution:

Method:

Select the section containing the low resolution test objects in the mini phantom. Perform a single transverse scan utilizing the same technique as high resolution.

Technique:

Kvp	130	mA	250	Seconds	1
-----	-----	----	-----	---------	---

Result:

Slice Thickness in mm	Resolution
1	0.5 %
2	0.5 %
3	0.5 %
5	0.3 %
10	0.3 %

Comment: Pass

8. mAs Linearity

Method

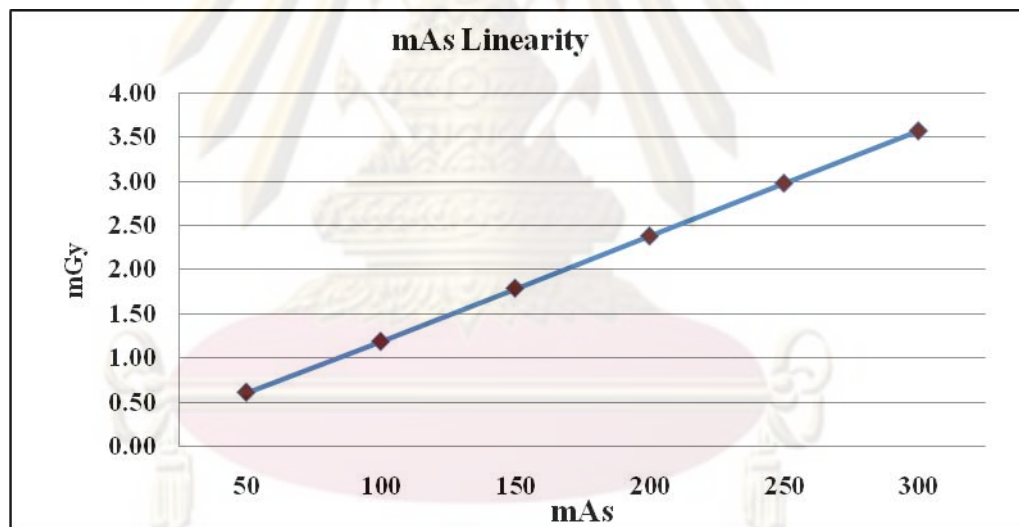
Set up the same as position dependence and insert 10 cm long pencil chamber in the center slot of the C.T. dose head phantom. Select the same kvp and time as used for head scan. Obtain four scans in each of the mA stations normally used in the clinic. For each mA station record the exposure in mR for each scan. Scans should be performed in the increasing order of mA. Compute mR/mAs for each mA setting.

Technique

Kvp	110	Sec	1	FOV	250
-----	-----	-----	---	-----	-----

Result:

mA	Exposure in mGy				mGy/mAs	C.V.
	Run 1	Run 2	Run 3	Run 4		
50	0.608	0.610	0.609	0.611	0.0122	1.000
100	1.183	1.187	1.187	1.189	0.0119	0.014
150	1.788	1.788	1.796	1.788	0.0119	0.003
200	2.378	2.386	2.379	2.385	0.0119	0.001
250	2.978	2.982	2.983	2.980	0.0119	0.001
300	3.561	3.578	3.584	3.576	0.0119	0.000



Comment: Pass

ศูนย์วิทยุทรัพยากร
จุฬาลงกรณ์มหาวิทยาลัย

SPECT/CT daily QC

The daily quality control program for CT and SPECT is regularly performed using water phantom for the study of CT image quality, kVp calibration, pixel noise and CT number values.

1. Water phantom

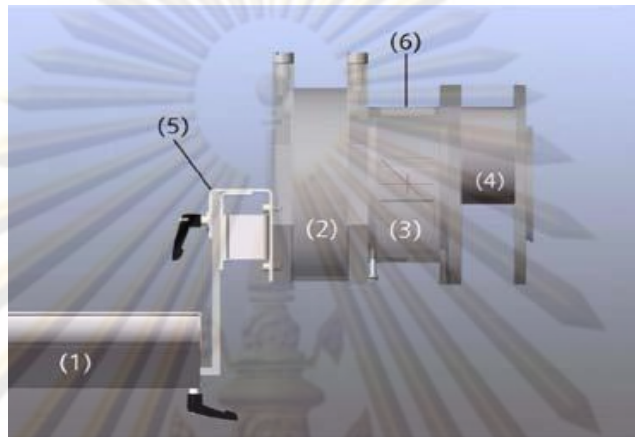


Figure VI Water phantom [(1) Patient table top, (2) Water phantom, (3) Slice thickness phantom, (4) Wire phantom, (5) Phantom holder bracket, (6) Reference marking]

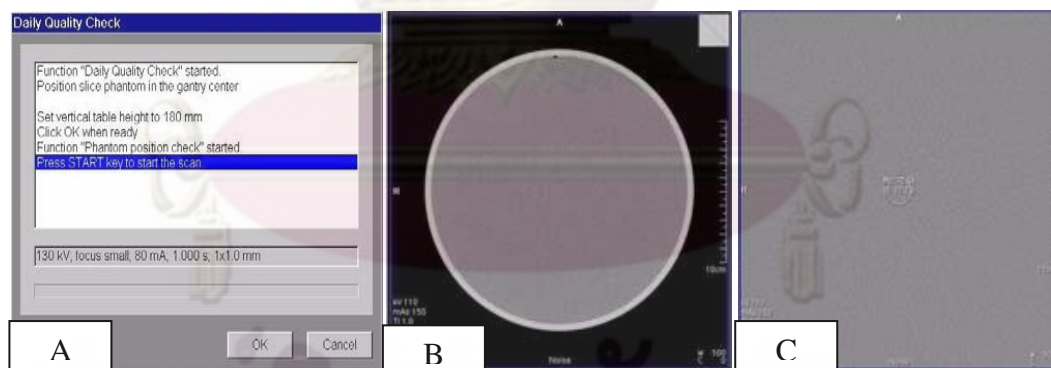


Figure VII kVp calibration set up (A) CT image of water phantom (B) ROI, mean CT value and Pixel Noise

ศูนย์เวชศาสตร์บูรณาการ
จุฬาลงกรณ์มหาวิทยาลัย

2. Quality control of SPECT/CT part of SPECT

The QC procedures can be performed automatically by using an internal point source of Tc-99m to check intrinsic uniformity and intrinsic tuning.

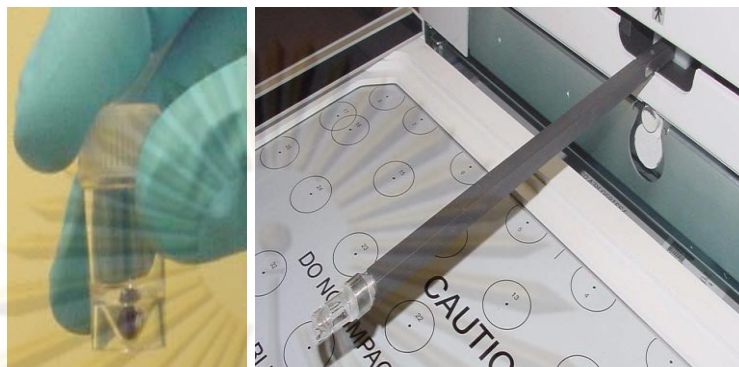


Figure VIII Point source vial (left) and source holder extended

Uniformity	CFOV	UFOV
Integrated	$\pm 2.0\%$	$\pm 2.5\%$
Differential	$\pm 1.5\%$	$\pm 2.0\%$

Table I Limit accept of intrinsic uniformity values

The results of the verification flood are acceptable if values are not exceeding from table I.

VITAE

NAME	Ms.Chayapa Kotewitee
SEX	Female
NATIONALITY	Thai
DATE OF BIRTH	May 25 1974
PLACE OF BIRTH	Roi-Ed, Thailand
INSTITUTIONS ATTENDED	Mahidol University, 2000: Bachelor of Science (Radiological Technology) Chulalongkorn University, 2010: Master of Science (Medical Imaging)
POSITION	Radiological Technologist
OFFICE ADDRESS	1873, Nuclear Medicine Division, Department of Radiology, King Chulalongkorn Memorial Hospital, Rama IV, Pratumwan, Bangkok, Thailand 10330 Tel. 02-2564283-84 ext. 103

ศูนย์วิทยุทรัพยากร
จุฬาลงกรณ์มหาวิทยาลัย